MIMO Channel Modelling and Performance Evaluations

Xiaoming Tu

Department of Electronic and Electrical Engineering

The University of Sheffield

A thesis submitted in partial fulfilment of the requirements for the degree of

Master of Philosophy

February 2018

Declaration

I hereby declare that except where specific reference is made to the work of others, the contents of this dissertation are original and have not been submitted in whole or in part for consideration for any other degree or qualification in this, or any other university. This dissertation is my own work and contains nothing which is the outcome of work done in collaboration with others, except as specified in the text and Acknowledgements.

Xiaoming Tu

February 2018

Acknowledgements

I would like to give my sincerely thanks to my supervisor, Prof. Jie Zhang and my second supervisor Dr. Wei Liu for their help and guidance throughout the course of my MPhil. I would also like to express my gratitude to the the members of the Communications Group, including Dr. Jialai Weng and Dr. Yang Wang who had many constructive discussions about my research project. I am also very grateful to the colleagues at Ranplan, including Dr. Jiming Chen, Dr. Hui Song and Dr. Zhihua Lai for their advices and suggestions that inspire me a lot.

Furthermore, I would like to give my huge thanks to Ranplan, my employer, who supported me on giving me extra time allowance on my research project and the free use of the commercial tool. I am also very grateful to Ranplan for providing measurement data without which the thesis could not have been completed.

Last but certainly not least, I would like to thank my family for their love and support throughout the period of this project including my parents Yuchai and Tanyuan, my wife Jinping. Thanks to my little children, Shihua and Jason who have given me so much happiness during this period so that I could still relax under high pressure from both the course and work.

Abstract

The demand on wireless networks with high throughput has grown heavily because of the increasing usage of data services. One of the key technologies to meet this requirement is the multiple-input multiple-output (MIMO) communication system, which improves the spectrum efficiency without too much investment on the infrastructure and new frequency spectrum.

In this theis, a new MIMO channel model is developed that is specific to real scenarios. This kind of channel models is more suitable for network planning tools because it takes the environment details into account. The first step of this work is a review on the state-of-the-art MIMO channel modelling and radio propagation modelling studies. It is then followed by a comparison of two propagation models that use different algorithms, i.e. ray optical and partial flow. The comparison leads to a decision that ray optical method is used for MIMO channel modelling in this thesis. After that, a spatial channel model based on a deterministic ray optical propagation model is proposed. The final MIMO channel model takes the polarisation and the Doppler effect in to account so that it can be used for MIMO systems with polarised antennas and moving objects as well. The model is used in a system level simulator and then validated in an indoor office building using measurement data.

It is concluded from this thesis that the chosen propagation model can be used for MIMO channel modelling, and the proposed MIMO channel model based on it is accurate and can be used for MIMO system design.

Table of Contents

List of Figures

List of Tables

List of Acronyms

Other Symbols

2D Two dimensions

3D Three dimensions

4G The Fourth Generation

5G The Fifth Generation

CSI Channel State Information

FDTD Finite-Difference Time-Domain

GA Genetic Algorithm

GO Geometric Optics

GTD Geometrical Theory of Diffraction

IRLA Intelligent Ray Launching

LOS Line of Sight

LTE Long Term Evolution

MIMO Multiple Input Multiple Output

mmWave Millimetre Wave

MR-FDPF Multi-Resolution Frequency Domain Partial Flow

RMSE Root Mean Square Error

SA Simulate Annealing

SCME Spatial Channel Model Extension

SCM Spatial Channel Model

SISO Single Input Single Output

SNR Single-to-Noise Ratio

TLM Transmission-Line Matrix

TTI Transmission Time Interval

UTD Uniform Theory of Diffraction

Chapter 1

Introduction

1.1 Background

With the rapid growth of mobile users, data rate and capacity of a wireless network has been much more demonding. The mobile data traffic requirement has been increased rapidly in the last few years. Voice phone calls cannot satisfy daily usage nowadays. Apps with data usages occupy the most time of people's daily use on mobiles. The 1000x (1000 times) growth in traffic acknowledged by the industry is in one decade [1]. On the industry's side, they need to be prepared for the challenge of meeting this requirement. There are many ways to meet the 1000x data challenge such as more spectrum, improving the spectrum efficiency and more small cells [2]. The most cost effective way of them is to improve the spectrum efficiency which can be achieved by using the multiple antennas (MIMO) technology. In the fifth generation (5G), or even in the fourth generation (4G) communications systems, the usage of multiple-input-multiple-output (MIMO) technology has grown a lot. Many industrial standards have already employed MIMO technology into their specifications to improve the capacity such as 3GPP E-UTRA (LTE) [3] and IEEE 802.11n [4].

Network planning and optimisation tools have become more and more important because they are essential for designing quality networks with high performance. Features provided by these tools enable the network designers to analyse the network performance before a network is actually deployed, and thus reduce the cost of maintenance afterwards. Channel models are needed by wireless network analyses for predicting the wireless communication channel state and enabling high level system simulations. New MIMO channel models are needed so that these planning and optimisation tools can still be used for simulations and then designing the new wireless systems.

Although many network designers design network based on their experience or the measurement data, they may need simulation results to make better decisions when they plan a new network or optimize an existing network. Accurate channel models will make the simulation results more reliable obviously.

The MIMO wireless communication channel has more than one antenna at both the transmitter and the receiver side. In dense environments, rich scattering exists between the transmitter and receiver. It improves the capacity of a MIMO channel by providing a new degree of freedom, i.e. space dimension in addition to the time dimension as compared to the conventional channel models. In conventional single-input-single-output (SISO) channels, multi-paths effect is considered as a negative effect to the channel quality but, in MIMO systems, they are utilized as providing another dimension to the channel.

The key elements of implementing a MIMO system are coding and signal processing. However, the propagation model and antenna configurations have deep impact on the performance as well. The channel capacity is primarily determined by the propagation conditions and antenna configurations. Many researches regarding the radio propagation models are targeting SISO channels. These models are not able to be applied to MIMO channels directly. Basically, the propagation condition between a pair of transmitting antenna and receiving antenna could be well modelled

by these models. When there are multiple antennas at either a transmitter or a receiver and they are closed enough, the mutual coupling effect is introduced and thus affects the radiation pattern of antennas. As a result, simply combining the impulse response of each pair of antennas is not accurate enough for MIMO channel modelling. Antennas and impulse response need to be considered together.

1.2 Motivation

An accurate MIMO channel model is helpful for quantifying the capacity of the system based on Shannon theory. If the capacity of a specific scenario is determined, the MIMO system could be optimized according to it and thus gains higher performance. Furthermore, accurate MIMO channel models have great help on investigating coding and signal processing techniques. Unlike SISO radio channels, MIMO channels rely more on specific scenarios because the additional degree of freedom that utilised by MIMO systems is the space.

Literature has shown [5] many different kinds of MIMO channel models. Some of them are based on statistics [6] [7]. Measurement campaigns are carried out to collect a large set of data so that the channel state information can be extracted from them based on statistical methods. Models are validated by complying the same statistical distributions with measurement data. Some other models are called physical models [8] [9]. They use relatively real assumption of the communication environment such as the position of the transmitter and receiver, as well as the environment database. The whole channel state is modelled by combining the physical radio with MIMO channel parameters. Since the environment has been taken into account, these models are usually more accurate in these environment as compared to the statistical models. This is why only physical models are studied in this project.

Not all radio propagation models are site-specific which means they are not specific to the environment. It models how the radio propagates in a free-space environment. In this project, these radio propagation models are categorised as empirical models. On the contrary, radio propagation models those are site-specific are categorised as deterministic models. Wireless network planning tools usually have the knowledge of the environment, i.e. an indoor network planning tool would have a three dimension (3D) geometrical structure that represents a building. In this case, deterministic models are more preferable because they could benefit from the existence of the building model. FDTD-like (Finite-Difference Time-Domain) [10] [11] and ray optical based algorithms [12] [13] are most widely used in deterministic models. These two algorithms both have they own advantages and disadvantages. An algorithm complexity comparison between these two methods [14] suggests that ray optical method is more suitable for single frequency analysis than FDTD methods. The combination of these two methods is also possible [15].

1.3 Thesis Contributions

In this thesis, a new physical MIMO channel model is proposed which is defined in the context of specific environments. It is so called as the site-specific channel model because the real environment data is taken into account. The environment is modelled in three dimensions (3D) so it reflects the building structures as they are in the real world. With this model, a deterministic radio propagation model is used to calculate the radio paths and their spatial variables. Then, the multipath components are recovered from these radio paths based on an algorithm that uses the delay time of each paths.

Since the MIMO channel model proposed is specific to individual environment, thus it is worth evaluating the performance in real scenarios. The proposed model is used in a system level simulator to evaluate the performance of the MIMO systems.

The simulations are based in real environment where measurement have been carried out. The simulation results are compared to the measurement data to demonstrate the accuracy of the model.

The remaining content of this thesis is organised as follows. In chapter 2, section 2.1 is an overview of the MIMO system. It gives the background of the problem that this thesis is trying to resolve. Section 2.2 is a categorization of the existing MIMO channel modelling methods. What MIMO channel models have already been developed and their differences are studied. In the last section 2.3, a review of different radio propagation models is given. What are those models and how they work are studied. In chapter 3, the first section 3.1 is a comparison between a ray-optical method and a numerical method for the radio propagation. It leads to a conclusion that the ray-optical method is used for the MIMO channel modelling in this thesis. The work in this section is published and presented at The Loughborough Antennas & Propagation Conference 2013. Section 3.2 is the main part that describes the model proposed in this thesis. Part of the content in this section is published and presented at General Assembly and Scientific Symposium of the International Union of Radio Science 2014. In chapter 4, the proposed model is used in a system level LTE network simulation to evaluate the network performance of a MIMO system in an indoor scenario. The simulation results are compared with measurements and discussed. In the last chapter 5, this thesis is concluded in the first section 5.1. The future work is described next in the last section 5.2.

During the study of this subject and writing up of this thesis, there are few papers published to conferences and a journal. They are listed in the appendix A.

Chapter 2

Review of Existing MIMO Channel Modelling

In this chapter, a review of the literature regarding the MIMO channel modelling will be described. Necessary background related to this project will also be described in details.

2.1 MIMO System Overview

Before we dig into the background of MIMO channel modelling, an overview of the MIMO system is worth noting.

In real radio propagation environments, the multi path effect is very common due to the rich scatter between transmitters and receivers. If there are multiple antennas being involved in both sides of the communication channel and the paths between different antennas could be resolved at the receiver, the system can encode multiple data streams into different transmitting antennas, thus improve the overall system capacity. This multipath communication is demonstrated in Figure 2.1. There are two antennas on both the transmitting side and receiving side. $Tx1$ has a reflected multipath component travelling to the $Rx1$ and $Tx2$ has another one travelling to the

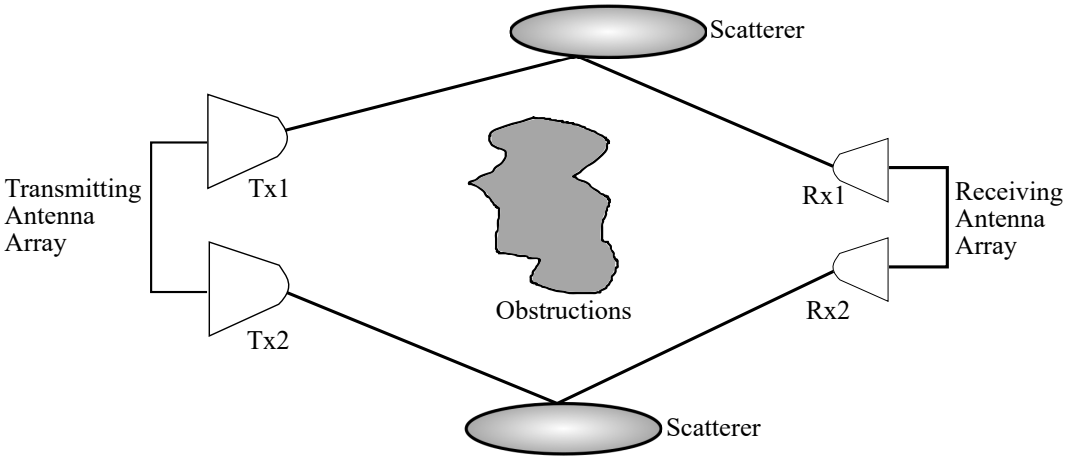

Figure. 2.1 Multipath propagation environment with two antenna arrays.

*Rx*2. If both transmitting antennas are sending different data streams simultaneously, the overall throughput could be improved [16] [17].

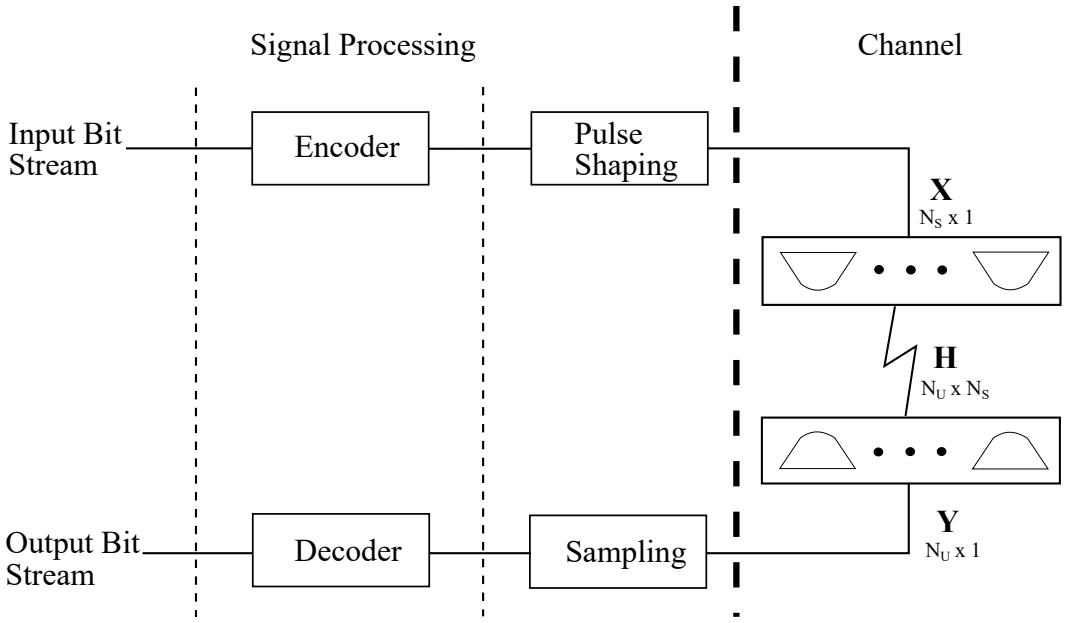

Figure. 2.2 Architecture of a generic MIMO system.

Layering is very important in the communication systems. The structure of a generic MIMO system is illustrated in Figure 2.2. It has several layers separated by dashed lines. The left three layers can all be categorized as the signal processing, so the structure is mainly divided into two parts [18]: 1) signal processing (left to the thick dashed line) and 2) the wireless channel (right to the thick dashed line).

In case of the downlink transmission, the system starts from the top-left with input symbols. These input symbols go through the signal processing layers first and are separated into different data streams. The transmitted signal on all antennas is denoted by a vector X with S elements. S is the number of transmitting antennas. The wireless channel is modelled by a matrix that is denoted by H and it has $U \times S$ elements. U is the number of receiving antennas. On the bottom side of the figure, the received signal is denoted by vector Y with U elements. It is processed by the signal processing layers again so that original input symbols can be recovered. The whole system is represented by following mathematical equation [18]

$$Y = HX + \eta \tag{2.1}$$

where η is additive noise produced by the channel. In this project, only the right part of Figure 2.2 is focused, which is to model the channel H.

Looking at the right part of Figure 2.2, the MIMO channel could be categorized into two types based on whether the antennas configurations are considered. One is called *Propagation Channel* which models the propagation channel itself. Another one is called *Radio Channel* that considers both antenna pattern and array configuration. Figure 2.3 shows the boundaries of the two concepts. These concepts are also used in [19] when *The Double-Directional Radio Channel* was proposed. In this project, the propagation channel is firstly studied in order to understand the physical properties of a wireless channel. Then radio channel is also studied so that the performance of MIMO systems could be evaluated.

Capacity

The capacity improvement of MIMO systems was originally investigated in [20] and [21]. At that time, there were not much studies about the channel characteristics, thus both of them assumed the channel to be additive Gaussian channel either with or without a fading model e.g. Rayleigh fading for indoor environment. If the

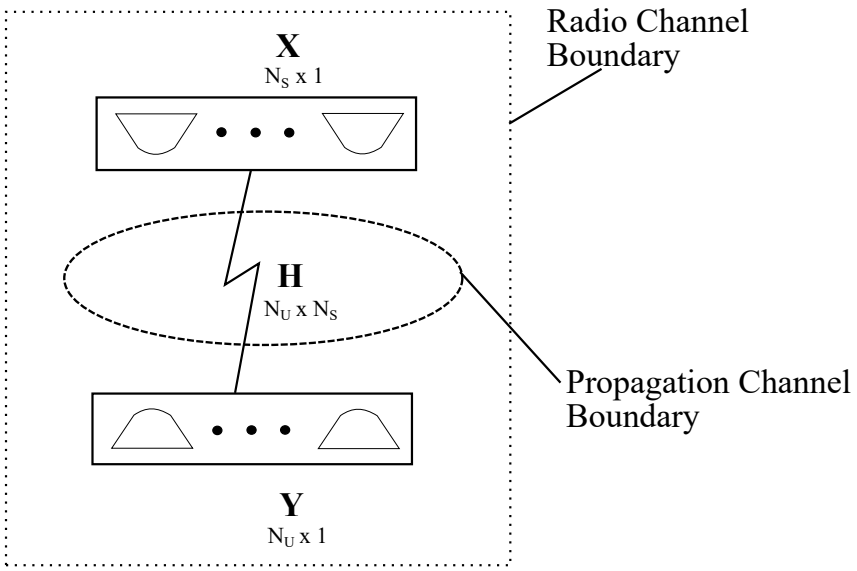

Figure. 2.3 Boundaries of radio channel and propagation channel.

magnitude of a channel follows Rayleigh distribution and the phase follows uniform distribution. The theoretical capacity of the MIMO channel with T transmitters and R receivers is defined as follows [22]:

$$C = B \cdot log_2 det(I_U + \frac{\rho}{S} HQH^H) \tag{2.2}$$

where H is the channel matrix, B is the bandwidth, $det(\cdot)$ indicates the determinant of a matrix, $(\cdot)^H$ is the conjugate transpose operation, I_R is $U \times U$ identity matrix, $\rho = E_s/N_0$ is the signal-to-noise ratio (SNR), and Q is the covariance matrix of input signals. It is also assumed that the channel state information (CSI) is known to the receiver.

From Equation. 2.2, it can be seen that signal-to-noise ratio ρ is decisive for the quality of the channel and therefore for the actual data rates. In a MIMO system, multiple antennas receive signals so the receiving signal power is higher than single antenna. This improves the signal-to-noise ratio directly and thus higher capacity. However in a real MIMO deployment, the capacity gain is much smaller than the theoretical limit, and it heavily depends on the operating environments that determine

radio channel characteristics [23]. The capacity analyses will be more accurate with practical channel characteristics. That is why the MIMO channel modelling has been more attractive and we come to this position where we propose our solution to solve this problem by using site-based deterministic approaches to model the MIMO channel. This is crucial in network planning in order to deliver the required capacity.

2.2 MIMO Channel Modelling

In this section, a study of literature regarding MIMO channel modelling is described in detail.

There are many ways to classify MIMO channel models [5], i.e., *site-based* or *generic models*, *time-varying* versus *time-invariant models*, *physical models* or *analytical models*. Generic models are categorized in contrast to those site-based models. Most of channel models are based on statistical analyses from measurement data, e.g., the authors used measurement data [24] to analyse a statistical multipath propagation model and match the capacity, pairwise magnitude and phase distribution and in [25], the authors propose a model that is very similar to our solution that is based on ray tracing algorithm as well but, the scatterings are randomly placed to model the environment. Both these two models can be categorized into physical models. The difference is where they take the locations of scatters from. The former uses a statistical distribution and the latter uses a geometrical database.

2.2.1 Correlation

In real world, the received signal is usually correlated because of the correction in space between antennas. It is proved in [26] that interlink correlation on the transmitter side indicated moderate to very high values even with large spatial separation of receiver antennas. This is because the distance between the transmitter

and receiver is usually far longer than the distance between antenna element on the transmitter side. The authors provide a method [27] for applying the correlation to the channel model which can be written as

$$\mathbf{H_{i',Corr.}} = c\mathbf{H_{i,Uncorr.}} + \sqrt{1-c^2}\mathbf{H_{i',Uncorr.}} \tag{2.3}$$

where $\mathbf{H_{i,Uncorr.}}$ and $\mathbf{H_{i',Uncorr.}}$ independently denotes other channel models that have not considered correlation, i.e. Kronecker model [6] and Weichselberger model [28], c is the correlation coefficient between the two channel models. The authors used the matrix collinearity as the correlation coefficient in the paper which can be written as

$$\mathbf{æ}(\mathbf{H_i}, \mathbf{H_{i'}}) = \frac{|\mathbf{tr}(\mathbf{H_i}\mathbf{H_{i'}^H})|}{\|\mathbf{H_i}\|_\mathbf{F}\|\mathbf{H_{i'}}\|_\mathbf{F}} \tag{2.4}$$

where H_i and $H_{i'}$ are the matrices to be compared, and $||\cdot||_F$ denotes the Frobenius norm of a matrix. It shows the degree of similarity of the subspaces of the compared matrices and ranges between zero and one, where zero means that the matrices are orthogonal to each other and one means that the matrices are similar [29]. It can be seen from these studies that the taking real environment into account in channel modelling is very important.

Based on the fact that correlation has important impact on the channel capacity, many models have been proposed to address this problem such as in [30], the authors proposed an exponential correlation matrix model to investigate the negative effect on the channel capacity.

The existence of correlations between received signals lead to that MIMO channel would not achieve the optimal capacity improvement as defined in Equation. 2.2. Therefore, modelling the physical radio propagation mechanism in multipath environment is also very important to minimize the negative effect of the MIMO

channel accuracy. Propagation models will be described in more details in Section 2.3.

2.2.2 Polarisation

Polarisation is another way to improve the capacity. It is similar as using physically separated antenna arrays. In polarised MIMO channels, signals are transmitted over different polarisation states. MIMO system based on polarisation diversity was firstly introduced in [31]. Then much work that take polarisation in to account have been done for MIMO systems. For example, a geometrical scattering model for dual-polarized MIMO fixed wireless channel was represented in [32]. An analysis and measurement of polarized MIMO system in 5.25G Hz has been discussed in [33]. These studies show the potential network performance improvement using polarised MIMO channels. In addition to this, another benefit of using this mechanism is that it is not restricted by the space of the deployment location, e.g. on radio towers. The polarisation diversity could be obtained using antennas with the same size.

A cross-polarised channel model is defined by the third generation partnership standards bodies (3GPP) as part of their spatial channel model (SCM) [34]. However, this model does not take the elevation spectrum into account. It is modelled in two dimension (2D). A recent investigation of utilising polarisation in MIMO systems is presented in [35], which does utilise the elevation spectrum and is modelled in 3D space.

By specifying the direction of the electrical field vector of radio waves, polarisation normally can be categorised into 3 types: linear polarisation, circular polarisation and elliptical polarisation. Linear polarisation is the most popular type of polarisation in wireless communication. The proposed MIMO channel model in this thesis supports antennas with linear polarisation.

2.2.3 Existing Channel Models

SCM [34], SCME [36] and WINNER [37] are defined by standard organisation, i.e. 3GPP. They are widely used and compared with other models. The different features and limitations of these three models are compared in details [38]. SCM was originally designed for outdoor scenarios. The three typical environments are suburban macro, urban macro and urban micro. It supports up to 2GHz which seems not quite useful for current network requirements. SCME is an extended version of SCM, it extends the frequency range of SCM to 5GHz. Both SCM and SCME are based on the spatial geometry of the transceivers to calculate critical parameters. In contrast, WINNER does not use spatial properties. The model parameters for WINNER are extracted from measurement campaigns.

In the SCM model, the model parameters are calculated from the spatial geometry of the transceivers thus it is important to understand the physical geometrical locations. The model's geometrical parameters are shown in Figure 2.4. There is one cluster n between the transmitter and the receiver. A cluster represents the obstacle on which a set of radio signals are reflected. Each radio signal in the set is called a subpath. On each path n, there are M subpaths all of which are reflected on the cluster n. Antenna arrays are used on both the BS and the MS side. There is one path component (black) from the BS to the MS through the cluster and one subpath m which transmits in the similar way as the main path shown in the figure. For the sake of clarification, only one path component and one subpath is shown. Dot line indicates the line-of-sight (LOS) path between the BS and the MS.

The final channel coefficients matrix is a U -by- S matrix of complex amplitudes. Each element of the matrix $h_{u,s,n}(t)$ means the complex amplitude of path n between

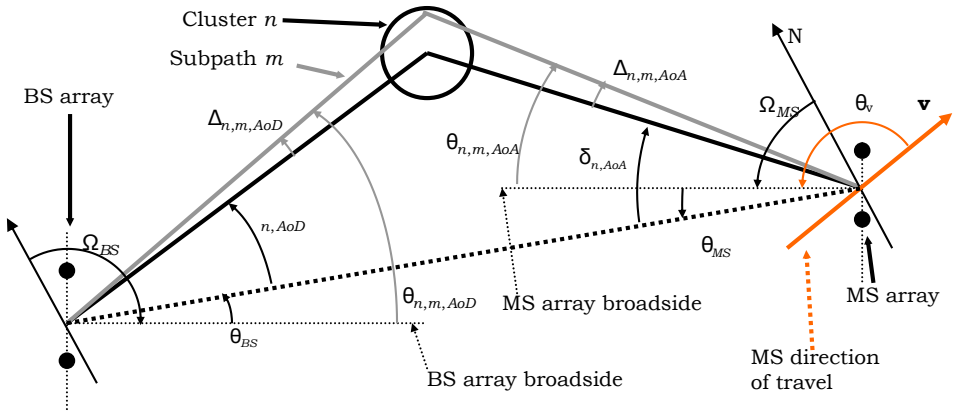

Figure. 2.4 Geometrical parameters in SCM (Reprinted from [34])

the antenna element u and s at time t and it is denoted by [34]:

$$h_{u,s,n}(t) = \sqrt{\frac{P_n \sigma_{SF}}{M}} \sum_{m=1}^{M} \left(\begin{array}{l} \sqrt{G_{BS}(\theta_{n,m,AoD})} \exp(j[kd_s \sin(\theta_{n,m,AoD}) + \Phi_{n,m}]) \times \\ \sqrt{G_{MS}(\theta_{n,m,AoA})} \exp(jkd_u \sin(\theta_{n,m,AoA})) \times \\ exp(jk\|v\|\cos(\theta_{n,m,AoA} - \theta_v)t) \end{array} \right) \tag{2.5}$$

where the parameters are explained in Table. 2.1.

Table 2.1 Parameters of the SCM channel coefficient

Symbol	Description
P_n	the power of the nth path
σ_{SF}	the lognormal shadow fading
M	the number of subpaths per-path
$\theta_{n,m,AoD}$	the AoD for the mth subpath of the nth path
$\theta_{n,m,AoA}$	the AoA for the mth subpath of the nth path
$G_{BS}(\theta_{n,m,AoD})$	the BS antenna gain of each array element
$G_{MS}(\theta_{n,m,AoA})$	the BS antenna gain of each array element
k	the wave number $2\pi/\lambda$ where λ is the carrier wavelength
$\Phi_{n,m}$	the phase of the mth subpath of the nth path
$\|v\|$	the magnitude of the MS velocity vector
θ_v	the angle of the MS velocity vector
s	the index of the transmitting antenna element ($s \in 0,1,...,S$)
u	the index of the receiving antenna element ($u \in 0,1,...,U$)
n	the index of the cluster (n predefined constant in [34])

The aim of the SCM model is to take the spatial properties of the environment into account of the channel model which seems to be closer to the reality. However, the clusters and paths are randomly generated at the beginning of the process.

Although this random process adds additional spacial information to the channel model, it does not reflect the real radio propagation scenario. In reality, there might be more complicated obstacles where a certain number of clusters are not enough to generate all the paths. The performance of the MIMO system relies on multipath and it may be affected a lot by this process. Thus, in this thesis, this random process is replaced by deterministic process. The geometrical structure of the scenario is described by 3D building models. A deterministic radio propagation model is used to calculate the spatial parameters of the radio paths in the building including path loss, angle of arrival, angle of departure and delay. In the next section, different radio propagation models are discussed at first. Then, two of them are compared later in more detail.

2.3 Radio Propagation Modelling

Radio propagation modelling plays an important role in wireless communications. It describes how radios propagate through the air and interact with obstacles. Empirical models and deterministic models are two major kinds of propagation models. Empirical models are not specific at certain environment. It is a generic representation of the radio propagation in a certain scenario, e.g. indoor office or urban scenario. On the contrary, deterministic models take environment details into account. These models need detailed description of the environment, i.e. 3D geometrical structure of the environment and material descriptions, thus they offer higher level of accuracy in the applied environments. the most widely used deterministic models are ray optical methods [39] and FDTD (Finite-difference time-domain)-like models. There are some other models sitting in between, e.g. HATA model [40]. It is not purely

independent of the environment. There are also some parameters in the model that represent the environment.

The simplest propagation model is the so-called Free Space path loss model. It is the power loss of the signal level when the radio propagates in free space where there are no obstacles between transmitters and receivers. Based on the inverse-square law, it is easy to write the power density S (also known as power per unit area at distance) in free space as the following equation.

$$S = \frac{P_t}{4\pi d^2} \tag{2.6}$$

where P_t is the transmitted power in Watt and d is the direct distance in metres between transmitter and receiving point. Assume that the receiving antenna is an isotropic antenna, it is known that its aperture to receive signal is $\frac{\lambda^2}{4\pi}$ where λ is the wave length in metre. Thus the received power P_r could be write as the following equation.

$$P_r = S\frac{\lambda^2}{4\pi} \tag{2.7}$$

The path loss in free space PL_{free} is given by the ratio of P_t over P_r which is:

$$PL_{free} = \frac{P_t}{P_r} = \frac{(4\pi d)^2}{\lambda^2} = \frac{(4\pi d f_c)^2}{c^2} \tag{2.8}$$

where f_c is the central frequency in Hertz and c is the speed of light in vacuum. By taking the logarithm of the above equation, the path loss can be derived as:

$$\begin{aligned} L_{free} &= 10\log_{10}(1000 \times \tfrac{(4\pi d f_c)^2}{c^2}) \\ &= 20log_{10}(d) + 20log_{10}(f_c) - 147.55 \end{aligned} \tag{2.9}$$

Note this derivation is only valid in the far field where electromagnetic energy assumed to be spherical spreading. The free space model is simplified to just take

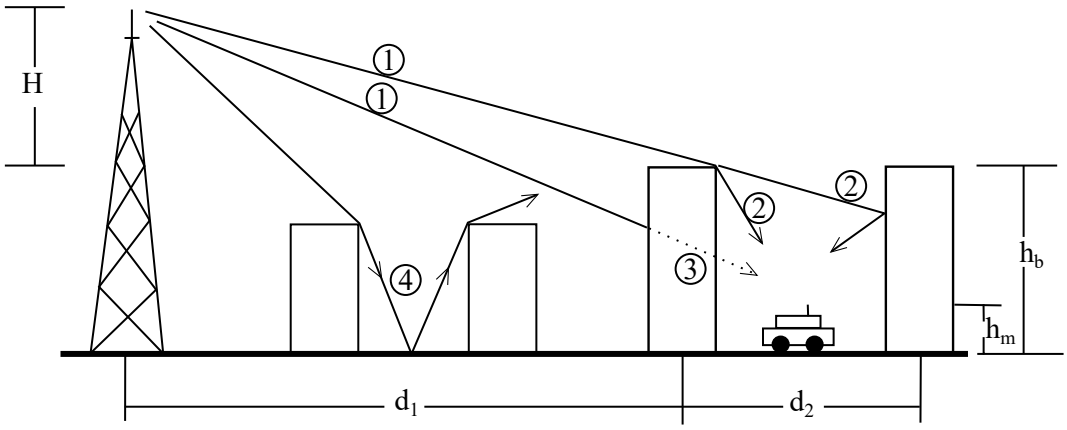

Figure. 2.5 Propagation in an urban area

the distance and frequency into account and does not have any considerations of environments, thus it is not suitable to provide accurate channel characteristics.

Another empirical propagation model was proposed by Joram Walfisch for urban communications in ultra high frequency bands [41]. The scenario that it is modelling is demonstrated in Figure. 2.5. The transmitter is located outside of the urban land area and the receiving antenna, which is on top of the car, is on a street between buildings. In this case, the significant paths that contributes to the main signal are path labelled ①. They reach the building in the front of the receiver, and then are diffracted or reflected to the receiver as labelled ②. The propagation may also penetrate through the building especially the building in the front of the receiver. This type of paths is labelled ③. Another type of paths that could reach the receiver is from the reflected paths by the ground between the buildings near the transmitter which is labelled ④.

In this model, the path-loss L_b between the transmitter and receiver is composed of two components:

$$L_b = L_0 + L_{ex} \tag{2.10}$$

where L_0 is the free-space loss and L_{ex} is defined as:

$$L_{ex} = 57.1 + A + \log(f_c) + 18\log(d_1) - 18\log(H) - 18\log[1 - \frac{d_1^2}{17H}] \tag{2.11}$$

and

$$A = 5\log((d_2/2)^2 + (h_b - h_m)^2) - 9\log(d_2) + 20\log(\tan^{-1}\frac{2(h_b - h_m)}{d_2}) \quad (2.12)$$

where f_c is the central frequency, d_1 is the distance between the transmitter and nearest building to the receiver, d_2 is the distance between two buildings, H is the height of the transmitter relative to the roof of the nearest building, h_b is the heigh of building, and h_m is the height of the receiver relative to the ground.

It is validated with measurements in [41] and the authors also suggested that more realistic models for diffraction could be incorporated into this model. However, it is only applied in outdoor environment and based on an assumption of a typical transmitting scenario thus it not suitable for providing propagation channel characteristics either.

The COST Hata Model is another empirical channel model. It is an output of COST 231 project [42]. This model is based on the Hata model. Both of them use four parameters: frequency f_c, distance d between the transmitter and the receiver, the height of transmitting antenna h_t, and the height of the receiving antenna h_b. The original Hata model has empirical formulations of the path loss L_{Hata} in **urban areas** as described in [40]

$$\begin{aligned} L_{Hata} = \quad & 69.55 + 26.16\log(f_c) - 13.82\log(h_t) - a(h_m) \\ & + (44.9 - 6.55\log(h_b))\log(d/1000) \end{aligned} \quad (2.13)$$

where frequency f_c is in MHz, h, h_m and d are in metres. $a(h_m)$ is the correction factor for vehicular receiving antenna height which differs on the size of the area and it is defined in Table. 2.2. In **suburban areas**, the path loss $L_{suburban}$ is defined as

$$L_{suburban} = L_b - 2(\log(f/28))^2 - 5.4 \quad (2.14)$$

And in **open areas**, it is written as:

$$L_{open} = L_b - 4.78\log(f)^2 + 18.32\log(f) - 40.94 \tag{2.15}$$

The Hata model is restricted to: frequency range $150 \sim 1500$ MHz, distance $1 \sim 20$ km, transmitting antenna height $30 \sim 200$ metre, and receiving antenna height $1 \sim 10$ metre.

Table 2.2 $a(h_m)$ defined in different scenarios

Scenario	Definition of $a(h_m)$
Medium small city	$a(h_m) = (1.1\log(f) - 0.7)h_m - (1.56\log(f) - 0.8)$
Large city ($f \leq 200MHz$)	$a(h_m) = 8.29[\log(1.54h_m)]^2 - 1.10$
Large city ($f \geq 400MHz$)	$a(h_m) = 3.2[\log(11.75h_m)]^2 - 4.97$

In [42], the Hata model is extended to the frequency band at 1500∼2000 MHz which is then renamed to the COST 231 Hata Model:

$$\begin{aligned} L_{Hata}' = \quad & 46.3 + 33.9\log(f) - 13.82\log(h_b) - a(h_m) \\ & + (44.9 - 6.55\log(h_b))\log(1000d) + C_m \end{aligned} \tag{2.16}$$

where $a(h_m)$ has the same definition with the Hata model and

$$C_m = \begin{cases} 0\text{dB} & \text{for medium sized city and suburban} \\ & \text{centres with medium tree density} \\ 3\text{dB} & \text{for metropolitan centres} \end{cases} \tag{2.17}$$

The COST Hata model also has the same restrictions as the Hata model except the frequency range has been changed to 1500∼2000 MHz. Even so, these models are not suitable for providing propagation channel characteristics because the multipath components are not considered. From here, it is obvious that the propagation that

are sufficient for MIMO channel modelling must take multipath components into account.

2.3.1 Ray Optical Method

The Intelligent Ray Launching (IRLA) model [43] [44] is a ray launching method based on ray optics, which models radio propagation by a discrete set of rays that are launched from the location of the signal source. Lots of rays are launched from the source location to every direction. Usually, a small angle is chosen for adjacent rays, but rays always diverge after reflections no matter what an angle is chosen. Figure 2.6a demonstrate this effect by showing the these rays in solid lines. After the second reflection, the divergence is very obvious. It is impossible to launch indefinite number of rays by a fixed angle interval in order to cover the entire area of interest.

There are many solutions to resolve this problem. An Impact Radius around the receiving point is introduced in [45]. All rays that intersects with this radius will contribute to the calculation of the total power at this location. Another method proposed in [45] is called Tube-Launching method, which launches three rays as a cluster for each direction. The method used in the IRLA model is by ray interpolation [46]. At each reflection point, more rays are launched from the reflection point so that the gaps between rays are filled. The dashed lines on Figure 2.6a demonstrate how these additional rays are filled. Note that not all re-launched rays are drawn in the figure. This method does require the calculation of reflection points for the new rays, which is the bottleneck of ray optics methods, because they are introduced after a reflection point is found [47].

The key radio propagation mechanisms that are considered by ray optical prorogation models are transmission, reflection, refraction and diffraction [48]. With the IRLA model, algorithms are implemented to model these mechanisms.

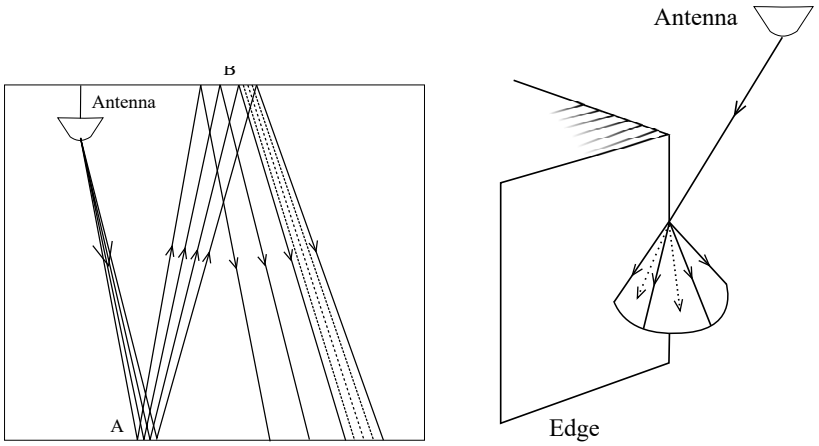

(a) Avoid ray divergence after reflection

(b) Diffracted rays with Keller Cone

Figure. 2.6 Ray traversal issues demonstration

The transmission loss is modelled the same as the Free Space path loss model, which is written as [49]

$$L_p = 20 * log(f_{MHz}) + 20 * log(d_{km}) + 32.24 \tag{2.18}$$

where f is the frequency in MHz and d_{km} is the distance from the receiver point to the transmitter in kilometre. Note the difference constant in the third term that is different than the Free-Space path loss model discussed earlier. This is because of the different unit used by f and d. During the transmission, the phase shift of each ray is also modelled as a function of distance:

$$\Delta\phi(d) = \frac{d}{\lambda} \tag{2.19}$$

When a ray intersect with an obstacle, the reflection, refraction and diffraction phenomenons are determined. Diffractions are determined only when the incident point is on an edge of the obstacle. Ray parameters are updated at each interaction point following the geometric optics (GO) theory. For the diffractions, ray parameters are updated following the principles defined by the geometrical theory of diffraction

(GTD) and uniform theory of diffraction (UTD). The shadowing effect of the radio propagations is very important. Diffracted rays in the IRLA model is modelled as a Keller Cone as illustrated in Figure 2.6b. Diffracted rays created by this method form a 3D cone to cover the area behind the edge. The previous method for dealing with the ray divergence effect is also used here to ensure all the areas are covered.

The shadowing is an important effect because it needs to be considered in network planning. However, it has not been modelled by the GO theory. In the IRLA model, the GTD is employed to model this effect. Rays are diffracted on the edge of obstacles following the GTD using a Keller Cone as illustrated in Figure 2.6b. These diffracted rays are launched from the diffraction point on the edge and they form a 3D cone. The method described previously for eliminating divergence effect is also used here to cover the entire area under the cone.

2.3.2 Numerical Method

Apart from the ray optics method, there is another category of deterministic radio propagation models using numerical method, e.g. finite-difference time-domain (FDTD) method [50] or the transmission-line matrix (TLM) method [51]. Both of them are numeric methods to solve the Maxwell's equations by discrete time and space steps in the time domain. These methods are used to solve the Maxwell's equations. There is comparison between the TLM method and the FDTD method in [51]. It has demonstrated that TLM has more accurate results than FDTD in some settings.

One of the disadvantages of both the FDTD method and the TLM method is the requirement of the high computation load. Another disadvantages of these methods is the need of the boundary condition in order to restrict the number of iterations. In [52], the multi-resolution frequency-domain partial flow (MR-FDPF) method is proposed which converts the wave approximation into the frequency domain. Thus

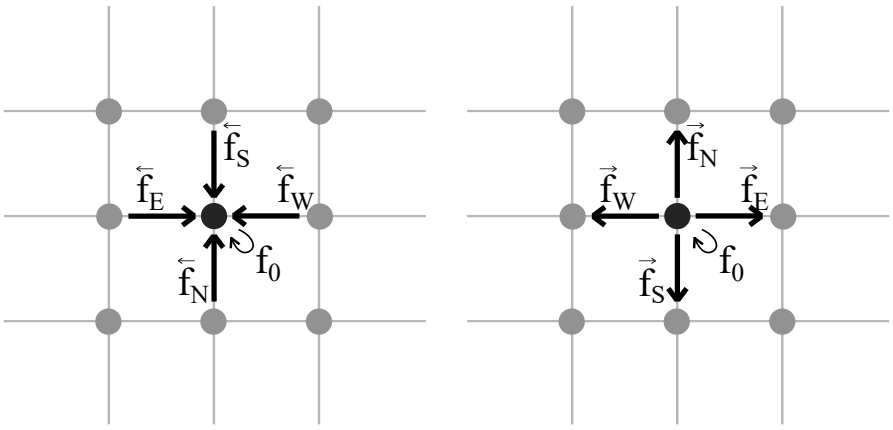

(a) Inward flows (b) Outward flows

Figure. 2.7 Flow directions on each pixel

boundary condition is no longer requirement. It also utilises the multi-resolution mechanism in so that higher performance is achieved compared to other methods.

The electric field is decomposed into four direction flows f_d and one additional stationary flow f_0. The direction flows f_d point to the four directions naming as $d \in \{E,W,S,N\}$. The stationary flow represents different dielectric media whose relative permittivity is not one. These flows are demonstrated on a 2D grid as seen in Figure 2.7.

The scattering equation of the MR-FDPF model at each location after transformation into the frequency domain leads to the following equation [52]:

$$\overrightarrow{F}(r,v) = \Sigma(r,v) \cdot \overleftarrow{F}(r,v) + \overrightarrow{S}(r,v) \tag{2.20}$$

where $F(r,v)$ is the inward directional flows vector. Over left arrow represents the inward flows and over right arrow represents the outward flows. $\Sigma(r,v) = \Sigma(r) \cdot e^{-j2\pi vdt}$ is the local scattering matrix at pixel r after transformation. $\overrightarrow{S}(r,v)$ is the electric field generated by the signal source. v is the central frequency. Note the stationary flow has been eliminated after transformation to the frequency domain. The complete local scattering matrix is defined as [52]

$$\Sigma(r) = \frac{1}{2n_r^2} \cdot \begin{pmatrix} 1 & \alpha_r & 1 & 1 & Y_r \\ \alpha_r & 1 & 1 & 1 & Y_r \\ 1 & 1 & 1 & \alpha_r & Y_r \\ 1 & 1 & \alpha_r & 1 & Y_r \\ 1 & 1 & 1 & 1 & \beta_r \end{pmatrix} \tag{2.21}$$

where $\alpha_r = 1 - 2n_r^2, \beta_r = 2n_r^2 - r, Y_r = 4n_r^2 - 4$ and n_r is the refraction index of the media.

By concatenating all inward and outward flows into a single vector F, the problem becomes a linear system [52]:

$$F = \Omega_0 \cdot F + S \tag{2.22}$$

where Ω_0 is the propagation matrix including the relationship of both the local scattering and neighbourhood.

Equation 2.22 is then solved by matrix geometric series and finally, the electric field at each location is computed directly by [52]

$$\Psi(r, v_0) = \sum_{d=\{E,W,S,N\}} \overleftarrow{f_d}(r) \tag{2.23}$$

The MR-FDPF model has been used in predicting radio coverage in indoor scenarios [53] and it is concluded from it that MR-FDPF is a fast and accurate way of predicting radio coverage.

2.3.3 Propagation Modelling for MIMO Channels

The MIMO channel provides higher capacity than the SISO channel because it utilises space. It means that the spatial characteristic of radio propagation is very important. The performance of MIMO channel models relies on the angle of arrival

(AoA) and angle of departure (AoD) information. These characteristics must be provided by the propagation model.

The TLM method models the radio wave in terms of flows on four directions at each position in the space. Different flows carry different amount of energy. At each position, the final receiving power is composed by combining the energy from different flows. The combining is repeated several times during the calculation. The direction could be tracked by analysing strong energy flows at the transmitter or the receiver position but it seems not be practical to define whether a flow is strong until the interactions have finished.

Chapter 3

MIMO Channel Modelling with IRLA

In this chapter, the methodology of using IRLA for MIMO channel modelling is described. It starts with a comparison between the IRLA model and the MR-FDPF method. Then, the detailed MIMO channel model with IRLA is discussed.

3.1 Comparison of IRLA and MR-FDPF

In this section, the performance of two radio propagation models are compared in terms of the speed and accuracy. Both of them are deterministic models. In this comparison, they are used to calculate the path loss in an indoor office scenario. Then the results are compared with the measurement data. There are two reasons for choosing the indoor office scenario. Firstly, both models have already been validated in the indoor scenarios [54] [11]. Secondly, the MR-FDPF requires very fine resolution and the computation resources needed for predicting an outdoor scenario is too much. Although both models have been combined for an outdoor to indoor coverage prediction [55], it is still confirmed that IRLA has a wider usage.

3.1.1 Introduction

The objective of this thesis is to develop a MIMO channel model in specific indoor scenarios utilising the deterministic propagation model. Given there are so many types of the propagation models, a study of the performance of the existing models is needed.

Both the IRLA model[43][44] and the MR-FDPF model[53][11] have been proven to be capable of predicting the signal coverage in specific scenarios with good agreement with measurement . Thus, the accuracy of both models is not a concern of this project. Since the proposed model will be applied in network planning tools, the performance in terms of both memory and computation resource usage has to be taken into account. It is more acceptable by the users of the planning tools if the results are given quicker. Personal computers used might not be powerful enough to carry out heavy computation load effectively.

In this project, an indoor office building located in Lyon, France is chosen as the testing scenario. Measurement was carried out in this building by the CITI laboratory at 3.4 Ghz where potential interference from WiFi networks does not exist[47]. The transmitter power was set to 20dBm. The material parameters for both models are calibrated using the same set of the measurement data assuming that both models will provide the best prediction after calibration. The performance of these two models are then compared and discussed.

3.1.2 Scenario and Measurement

The first floor of the target building is used in this test. Figure 3.1 illustrates its floor plan. As seen from the figure, there is a long L-shape corridor on this floor and 28 rooms around it. This is a typical indoor office scenario. The building is built up with concrete for its out walls. Bricks are used to separate rooms. Wood and glass are used for doors and windows respectively. The transmitter ('Tx') is placed in a

Figure. 3.1 Floor plan of the second floor

room on the left side as show in the figure and it is single omni-directional antenna with 0dBi gain. Different materials are drawn with different colours and widths.

The measurement is done using a spectrum analyser [56] and the received signal level is measurement at 70 locations. The transmitting power of the transmitter is set to 20 dBm. The spectrum analyser has a sensitivity of -141 dBm/Hz. Because the measured bandwidth is set to 300 KHz, the sensitivity of the spectrum analyser described in dBm is $(-141+10\log(3*10^5)) \approx -86dBm$. In this case, the measured signal level less than $-86dBm$ would have extra noise. The locations where the measured signal level is higher than this value are ignored. The remaining data are used in the calibration process.

3.1.3 Calibration of Materials

In this project, all material parameters used by both models are calibrated assuming they are providing the best predictions after calibrating material parameters. The

IRLA model relies on the empirical loss when different radio propagation phenomenons occur, i.e. transmission loss, reflection loss, refraction loss and diffraction loss. However, in the MR-FDPF model, the single refraction index and attenuation coefficient are used. Usually, material parameters are physical attributes of materials and should not be changed, but the material parameters used by these models may vary in different environment because of the humidity or the thickness of building walls.

The calibration process is a process of finding the best candidate value of variables so that the defined target function (also know as the fitness function) is minimised [55]. The software packages that implement these two models have different calibration algorithms though the fitness function used by them are the same, which is the root mean square error (RMSE) of the predicted signal level and measured signal level. Thus the optimisation problem is the same which is denoted as:

$$\min_{m_i \in R} \sqrt{E[(P(m_i) - M)^2]} \tag{3.1}$$

where m_i are the material parameters, R is the set of real numbers, $E[\cdot]$ is the expectation operator, $P(m_i)$ is the predicted signal level at each measured location and M is the measured signal level vector.

The genetic algorithm (GA)[57] is used by the MR-FDPF model to find the best candidate value of its material parameters. These parameters of each material type are composited as a chromosome which is a concept of GA representing a solution. Chromosomes of each material are generated in each generation of GA randomly. These material parameters are used to evaluate the fitness function. Chromosomes with better fitness result are chosen to reproduce the filial generation. The iterations stop after a large number of iterations. In the IRLA model, the optimisation algorithm used is different, which is called simulate annealing (SA) algorithm [58].

In the calibration process, the same set of the measurement data are feed to both propagation models so they could adjust the material parameters accordingly. Once it is done, it is assumed that the material parameters are correct and both model should give the best prediction results. The calibration result of the both models are shown in Figure 3.2. For the MR-FDPF model with GA algorithm, the RMSE of the predicted signal level and measured signal level is reduced down to 5.38 dB from 10.46 dB. For the IRLA model, it is reduced to 6.3 dB from 7.83 dB.

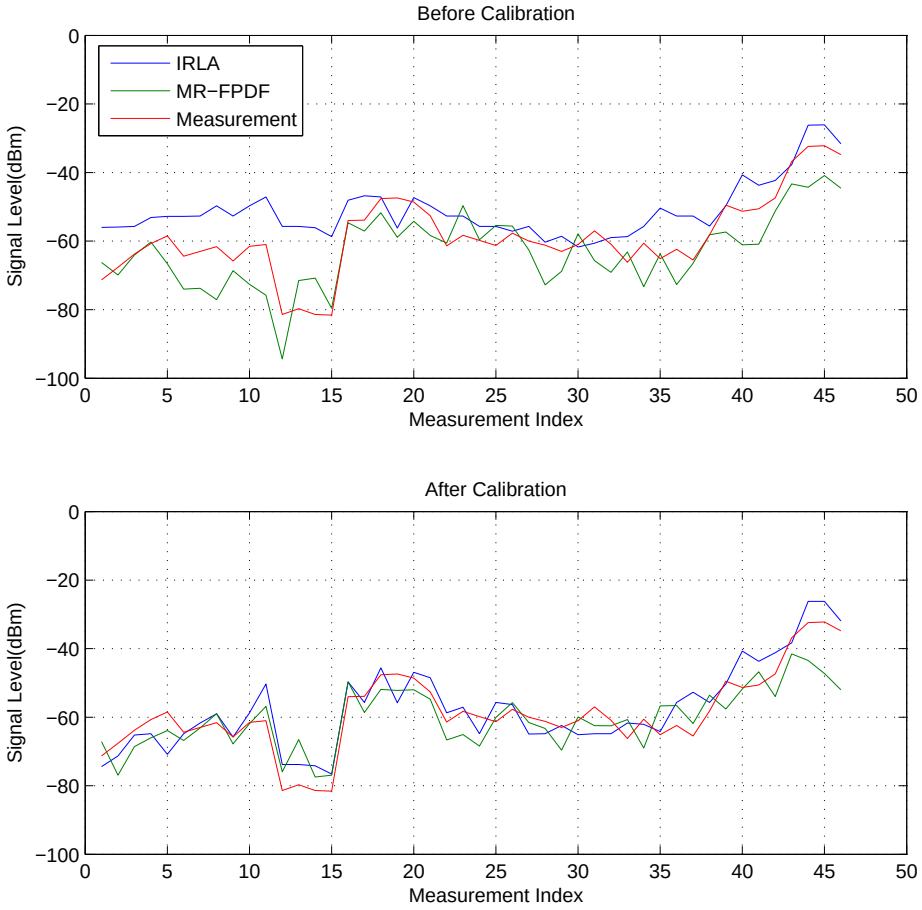

Figure. 3.2 Comparison between signal level and measurement using the IRLA model and the MR-FDPF model above.) before calibration; below.) after calibration.

3.1.4 Simulation Results Comparison

Both propagation models are susceptible to resolutions, thus a number of predictions for signal level are performed at different resolutions for both propagation models. The performance of them at these resolutions are compared respectively.

Figure 3.3 shows the predicted signal level coverage from two propagation models at 0.1 metre resolution. The result from the IRLA model is shown on the top while the the result from the MR-FDPF model is shown on the bottom. For the IRLA model, the maximum number of reflections and transmissions of rays are set to 9, and the path loss limit is set to 280 dB.

The computation time and memory consumption for each run are recorded in Table 3.1. The simulations are run on a Intel i7-3610QM laptop with 8 GB memory. Overall, the IRLA model uses less memory but more computation time than the MR-FDPF model. This difference is more significant in finer resolutions, e.g. 0.1 metre. It is worth noting that the IRLA model predicts the signal level in 3D while the MR-FDPF model predicts in 2D only.

Table 3.1 Computation Resource Comparison at Different Resolutions

	0.1m	0.2m	0.3m	0.5m
Memory (IRLA)	1.02GB	205MB	94MB	42MB
Memory (MR-FDPF)	1.9GB	448MB	201MB	82MB
Time (IRLA)	9min44sec	43sec	8sec	3sec
Time (MR-FDPF)	38sec	8sec	4sec	2sec

Both models are capable of predicting the signal coverage as proven by the other work. In this project, the accuracy is also compared in this specific scenario. The RMSE between the measurement data and predicted signal level calculated at different resolutions are recorded in Table 3.2. Both models have shown very good results when the resolution is under 0.3 metre. However, the RMSE calculated by the MR-FDPF model becomes large at high resolutions. The reason is that it is

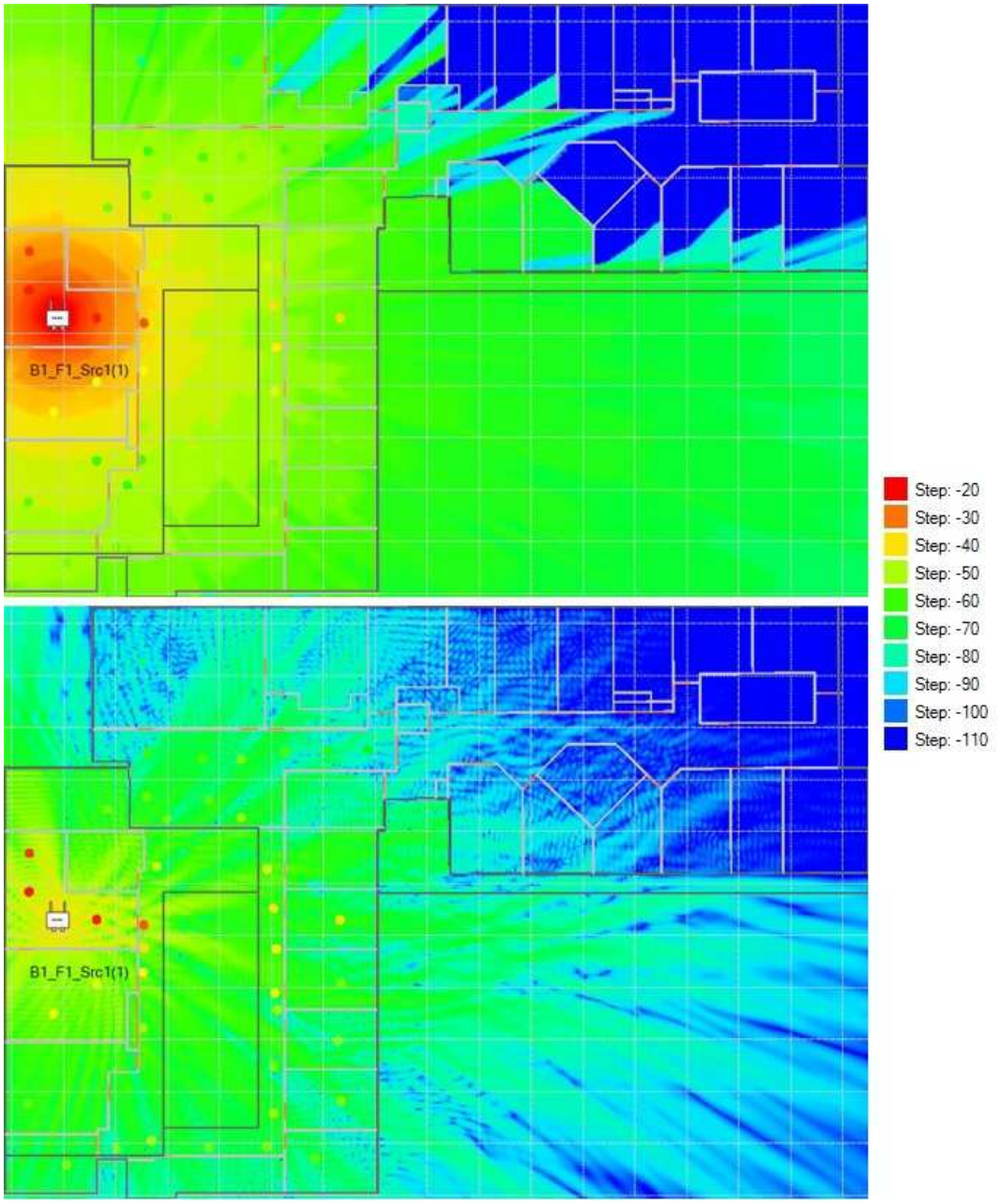

Figure. 3.3 Signal level coverage comparison with measurement data. The circles on both sub figures represent the measurement point. top.) Predicted by the IRLA model. bottom.) Predicted by the MR-FDPF model.

constrained by the resolution. The suggested resolution is $\leq \lambda/6$ [52] that is 1.5 centimetre in this case and it is far less than the finest resolution used here.

Linear regression is used to statistically analyse the predicted results from two propagation models. The best fitting linear polynomial is found to be $f(x) = 1.232x +$

Table 3.2 RMSE of the Best Signal Level Comparison at Different Resolutions

	0.1m	0.2m	0.3m	0.5m
RMSE (IRLA)	5.1dB	5.4dB	5.8dB	6.9dB
RMSE (MR-FDPF)	6.5dB	6.8dB	8.6dB	11.5dB

13.71, where $f(x)$ represents the predicted signal level from the IRLA model and x is the predicted signal level from the MR-FDPF model. Both the predicted results and the fitting polynomial is shown in Figure 3.4. Replacing $f(x)$ with x, it is possible to calculate x which leads to -59 dBm. This value indicates the point from where the two sets of the predicted results starts deviating. Given that the slop of the polynomial is greater than 1, when signal level is lower than -59 dBm, the MR-FDPF model gives more optimistic predictions. The same result can be observed from Figure 3.4.

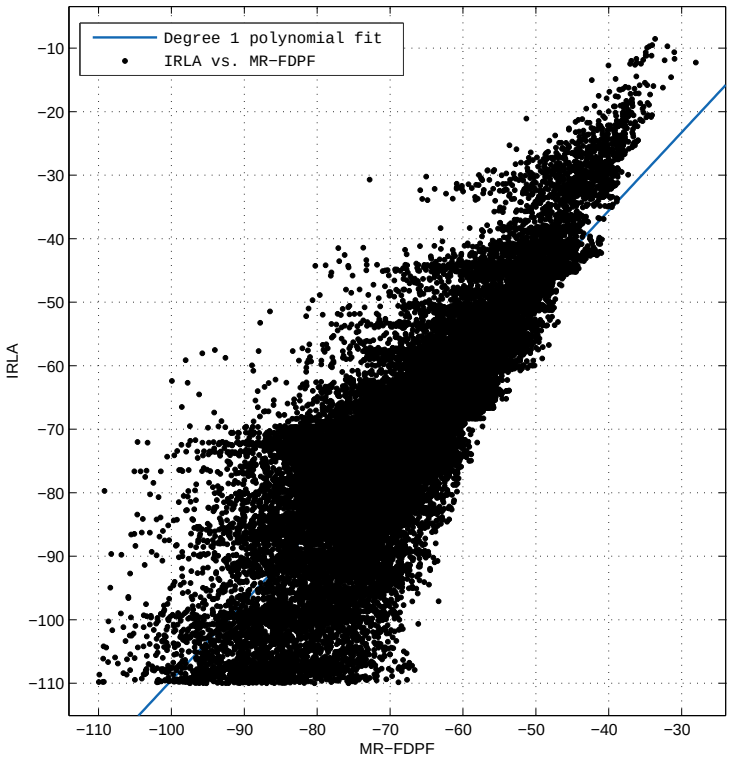

Figure. 3.4 Prediction results and best fitting linear regression

3.1.5 Summary

In this section, two kinds of propagation models, ray optical-based model and partial flow-based model, are used to predict the signal coverage in an indoor office building. The predicted signal level are compared with measurement data and they are also compared with each other.

The comparison on coverage prediction suggests that both models have a good prediction on the coverage at fine resolutions. While at dense resolutions, e.g. 0.5 metre, the IRLA model gives much better result than the MR-FDPF model. This is because the MR-FDPF model has higher requirement on the resolution. The suggested resolution is $\lambda/6$ where λ is the wave length [52].

The comparison on computation resource usages suggests that the IRLA model is more efficient than the MR-FDPF model. The MR-FDPF model uses more memory when compared to the IRLA model. It is almost twice of what the IRLA model uses. It is worth to mention that the MR-FDPF model uses much memory on caching the local scattering matrix at each pixel and it is not changing between different predictions in the same scenario. This can be a benefit for network planning tools because further predictions are much quicker. Another interesting fact is that the MR-FDPF model is not sensitive to the complexity of the environment, while for the IRLA model, computation load increases largely when the environment becomes more complicated.

It can be seen that both model are capable of predicting coverage in indoor scenario. For small office buildings with complex building structure, the MR-FDPF model is recommended. However, for the other scenarios, the MR-FDPF model would not be able to perform as well as the IRLA model. The criteria for choosing between these two models are not fixed. It depends on the signal frequency, the power and the available memory of the computer.

3.2 MIMO Channel Modelling

In this section, the MIMO channel model is proposed using the IRLA model. This model is explained as follows.

3.2.1 Introduction

With the fast development of smart city and indoor localisation systems, more and more cities and buildings have been modelled by 2.5D/3D geometrical models. Currently, most MIMO channel models are proposed for general scenarios e.g., urban, LOS or NLOS, and they are based on statistical analyses or measurements. If the environment models could be taken into account, the designed channel models will be more accurate and fit to their targeting scenarios.

Given such an environment and the expected antenna configurations, how to generate the specific MIMO channel coefficient matrix so that the network could be optimized before it is finally deployed is the primary target of this project. According to the mathematical description of the MIMO system model, the task is to find the channel matrix H for a specific scenario.

For a MIMO system that has S transmitting antennas and U receiving antennas, the time-variant channel coefficient is represented by

$$H(t) = \begin{pmatrix} h_{1,1}(t) & \cdots & h_{1,S}(t) \\ \vdots & \ddots & \vdots \\ h_{U,1}(t) & \cdots & h_{U,S}(t) \end{pmatrix} \tag{3.2}$$

where $h_{u,s}(t)$ is the complex channel coefficient of the sth transmitter antenna and the uth receiving antenna at time t. Each element in the matrix represents the channel state of a communication path at a specific moment.

In network planning tools, the range of the area where the network performance is interested is wide and it usually covers the entire scenario. That means, this channel matrix needs to be calculated everywhere.

The IRLA model that has been described previously uses a rasterization mechanism to speed up the calculations [59]. The side effect of this mechanism is that it ignores the difference between two antenna pairs if the transmitting antennas and the receiving antennas of each pair are in the same rasterization cells. In indoor scenarios, the resolution is recommended to be 20cm for IRLA [47]. This is longer than the wavelength of a 2.4GHz WiFi network. In outdoor scenarios, where the resolution can be 2 to 5 metres, all antennas of an MIMO antenna array will be in the same rasterization cell. Multipath between each pair of the antennas will be the same. The correlation between each communication path becomes too hight to get any benefit of using multiple antennas.

Usually the spacing between antennas on the antenna array is relatively small, e.g. few wave lengths, and thus, it is fair to assume that all antennas would have the same multi paths. This means the power, AoA or AoD can be considered as the same at each antenna but the phase is different. This can be computed based on the geometrical position of antennas.

In the remaining of this section, a method is proposed to estimate the channel state for each pair of antennas so that IRLA could be used in MIMO channel modelling.

3.2.2 Overview

The overall procedure of this method is shown as a block diagram in Figure 3.5.

In the environment modelling stage, the input data for the proposed MIMO channel model is prepared including the 3D building model and configurations of the transmitters. These data are passed to IRLA which will calculate the radio propagation rays. Once this calculation is finished, the proposed method will collect

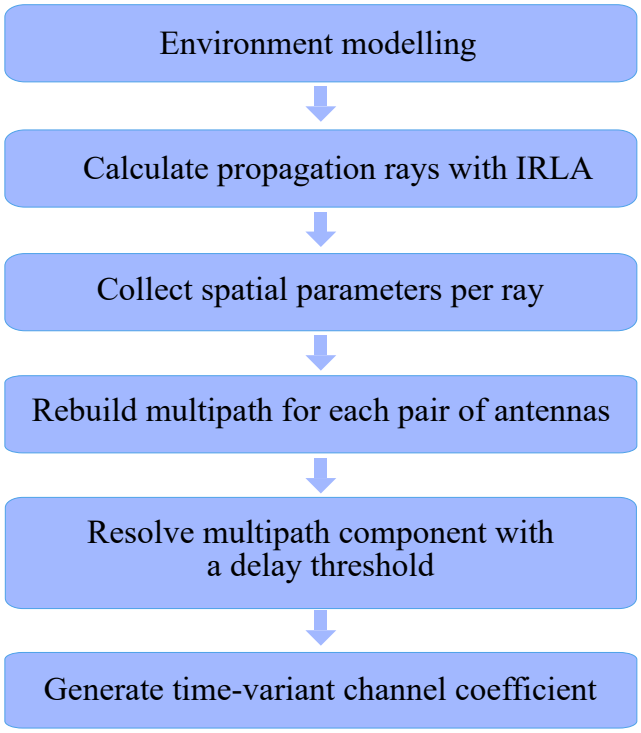

Figure. 3.5 Overall procedure of the channel estimation

the spatial channel parameters for each ray, including path loss, delay, AoA and AoD from the IRLA output. After that, the multipath components between each pair of the transmitting and receiving antenna is derived from the previous rays. Finally, the channel coefficient of each sub channel is calculated.

With this MIMO channel model, the channel state between the transmitter and each location in the building could be calculated. This allows other system level simulators to evaluate the network performance. The proposed model requires lots of computation resources especially for the IRLA to generate propagation rays at each location. Thus, for the larger scenarios, e.g. outdoor scenario, dense resolution is recommended to limit the computation time. As the IRLA model relies on the transmission, reflection and diffraction loss of building materials [54], a calibration process may needed in the second stage so that the these parameters are realistic. It is also worth noting that the proposed model can only be used for linear and circular

antenna arrays at the moment. For the other MIMO antenna configurations, further work is needed.

3.2.3 Spatial Parameters per Ray

In this stage, spatial parameters of each ray is calculated. With IRLA, thousands of rays are generated between two locations depending on the calculation configurations, e.g. number of reflections.

Each ray from the IRLA model is characterised by its own spatial parameters including path loss, delay, AoA and AoD. Some other parameters like power and delay also belong to spatial parameters because they are determined by the route of the ray. nth ray is a collection spatial parameters and is denoted as R_n.

$$R_n = \{P_n, \tau_n, \theta_{n,AoA}, \theta_{n,AoD}\} \tag{3.3}$$

where P_n is the power, τ_n is the delay, $\theta_{n,AoA}$ is the angle of arrival and $\theta_{n,AoD}$ is the angle of departure of nth ray.

All these rays are independent. They are caused by the four major phenomenons of radio propagation including reflection, refraction, transmission and diffraction. All these physical phenomenons have been modelled by the IRLA model.

The multipath component between two locations is a group of rays which written as

$$MP = \{R_n\}, n \in \{1, 2, ..., N\} \tag{3.4}$$

where N is the total number of rays in a single multipath component.

3.2.4 Rebuild Multipath

If a 2-by-2 antenna array is taken as an example, there are four sub channels for communications. Two transmitting antennas may be in the same rasterization cell.

Same happens for the receiving antennas. In this stage, rays of a multipath component between each pair of the transmitting antenna and receiving array, $MP_{u,s}$, is rebuilt from the single set of multipath from previous stage.

Based on different configurations of antenna arrays, rays between each antenna pair have different phase shift. A simple phase model is used to determine the phase shift for each ray. The phase of ray n between transmitting antenna u and receiving antenna s is a sum of the phase shift at both sides, and it is denoted as

$$\phi_{u,s,n} = \Delta\phi_{s,n} + \Delta\phi_{u,n} \tag{3.5}$$

For a linear antenna array with ΔD antenna spacing, the phase shift at both sides are defined as [60]

$$\Delta\phi_{s,n} = \frac{2\pi}{\lambda} s\Delta D \sin(\theta_{n,AoD} - \theta_{dir,BS}) \tag{3.6}$$

$$\Delta\phi_{u,n} = \frac{2\pi}{\lambda} u\Delta D \sin(\theta_{n,AoA} - \theta_{dir,UE}) \tag{3.7}$$

where $\theta_{dir,BS}$ is the direction of the transmitting antenna array, $\theta_{dir,UE}$ is the direction of the receiving antenna array, and the λ is the wavelength.

For a circular antenna array with ΔR as its radius, the phase shifts at both sides are defined as [60]

$$\Delta\phi_{s,n} = \frac{2\pi}{\lambda} \Delta R \sin(\theta_{n,AoD} - s\theta_{dir,BS}) \tag{3.8}$$

$$\Delta\phi_{u,n} = \frac{2\pi}{\lambda} \Delta R \sin(\theta_{n,AoA} - u\theta_{dir,UE}) \tag{3.9}$$

After that the phase for each ray is determined for each pair of antennas, the ray expression becomes

$$R_{u,s,n} = \{P_{u,s,n}, \tau_{u,s,n}, \theta_{u,s,n,AoA}, \theta_{u,s,n,AoD}, \phi u, s, n\} \tag{3.10}$$

3.2.5 Resolve Multipath Component

In the IRLA model, lots of rays may travel through the same route to the receiver. This happens because of the rasterization mechanism and fundamental theory of ray-tracing algorithm. Not all of these rays are independent communication channels. Thus, rays from the same route need to be identified and grouped as a single path. Figure 3.6 demonstrates this phenomenon. More than one ray travel through a path over cluster *A*. These rays are treated as one path in the MIMO channel.

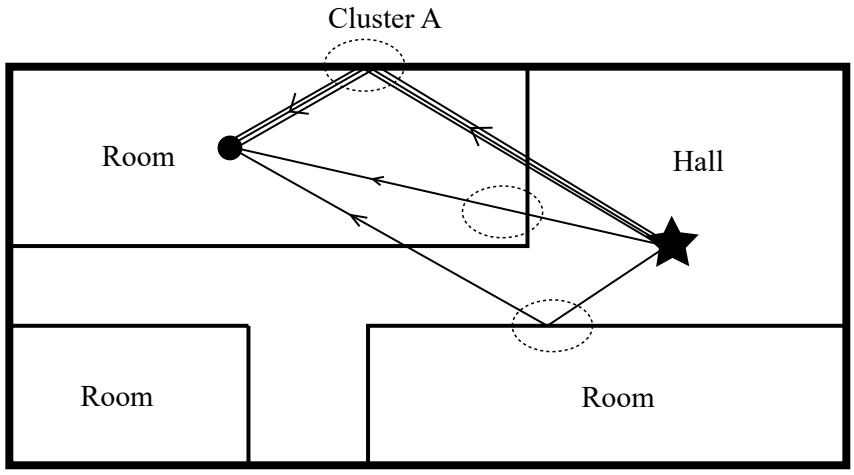

Figure. 3.6 Demonstration of rays from three paths

This is accomplished by aggregating rays based on their delay. Rays with similar delay are assumed to travel through the same path which has the same set of parameters but with different values. All rays are sorted by their delay $\tau_{u,s,n}$. Starting from the first ray up to the ray whose delay exceeds the delay threshold τ_{th} are grouped together and they are treated as a single MIMO path which is denoted by $R_{u,s,m}$. The delay of new path $\tau_{u,s,m}$ is determined by the earliest arriving ray. That means path $R_{u,s,m}$ has the shortest delay of all rays in its group.

$$R_{u,s,m} = \{R_{u,s,n} \mid \tau_{u,s,n} - \tau_{u,s,m} < \tau_{th}\} \tag{3.11}$$

where $\tau_{u,s,k}$ is the delay of ray $R_{u,s,n}$, $\tau_{u,s,m}$ is the delay of the earliest arrived ray in mth path group, τ_{th} is a constant threshold of the delay resolution. After the aggregation, all rays are regrouped into a total of M MIMO paths.

The power of all rays of the same path are summed up. Due to the side effect of the above aggregation method, power of each path may vary a lot and has large impact on reflecting the result of the MIMO channel. To eliminate this, the power of each path is divided by the total power of all paths. It is defined as

$$P_{u,s,m} = \frac{\sum_{n=1}^{N_m} P_{u,s,n}}{\sum_{n=1}^{N} P_{u,s,n}} \tag{3.12}$$

where N_m is the total number of rays in the new mth MIMO path.

The multipath component between each pair of the transmitting and receiving antenna $MP_{u,s}$ has now been rebuilt.

3.2.6 Generate Channel Coefficient

In this stage, given the physical channel parameters of each path between each antenna pairs, the channel coefficient matrix is generated. Each element of this channel coefficient matrix is a complex quantity.

If only the antenna gain is considered, the channel coefficient matrix for the mth multipath component is a sum of gains from each rays, which is written as [34]

$$h_{u,s,m} = \sqrt{\frac{P_{u,s,m}}{N}} \sum_{m=1}^{N_m} G_{(ant)} \tag{3.13}$$

$$G_{ant} = \sqrt{G_s(\theta_{n,AoD}) + G_u(\theta_{n,AoA})} \exp(j\phi_{u,s,n}) \tag{3.14}$$

where $G_s(\theta_{n,AoD})$ and $G_u(\theta_{n,AoA})$ are the pattern gain of transmitting antenna and receiving antenna respectively.

Mobiles devices are usually so small that antennas cannot be separated enough to avoid mutual coupling. The antennas spacing is much less than the half wavelength. It is very likely that polarised antennas will be used to implement multiple antennas. In this case, the gain from antenna becomes [34]

$$G_{ant} = \sqrt{G_s(\theta_{n,AoD}) + G_u(\theta_{n,AoA})} G_{polar} \exp(j\phi_{u,s,n}) \tag{3.15}$$

where

$$G_{polar} = \begin{bmatrix} \cos(\psi_s) & \sin(\psi_s)\cos(\phi_{n,AoD}) \end{bmatrix} \begin{bmatrix} 1 & r_n \\ r_n & 1 \end{bmatrix} \begin{bmatrix} \cos(\psi_u) \\ \sin(\psi_u)\cos(\phi_{n,AoA}) \end{bmatrix} \tag{3.16}$$

where ψ_s and ψ_u are the polarisation angle of the transmitter antenna s and receiver antenna u.

When the mobile devices are moving, the communication distance between the transmitter and the receiver becomes shorter. Each radio wave takes less time to travel. Thus the received frequency is different than the transmitted frequency. This phenomenon is called Doppler Effect (or Doppler Shift) [48].

Assuming the movement of the mobile device is described by the vector $\mathbf{v}$, the channel coefficient becomes [34]

$$h_{u,s,m}(t) = \sqrt{\frac{P_{u,s,m}}{N}} \sum_{m=1}^{N} \left(G_{ant} \times G_{doppler}(t) \right) \tag{3.17}$$

where $G_{doppler}(t)$ is the gain caused by Doppler Effect at t moment and it is defined as

$$G_{doppler}(t) = \exp(j\frac{2\pi}{\lambda} \|\mathbf{v}\| \cos((\theta_{n,AoA} - \theta_{\mathbf{v}})t)) \tag{3.18}$$

The moving direction $\theta_{\mathbf{v}}$ is relative to the line-of-sight direction as demonstrated in Figure 2.4 and the speed $\|\mathbf{v}\|$ is in metre per second.

3.2.7 Summary

A new MIMO channel model is proposed in this section. The new model takes the advantage of the IRLA model that has good estimations of channel parameters. A simple phase model is used to generate phase shift for each path between each pair of antennas. Multipath components for every antenna pair are also rebuilt from a single set of multipath components. The new model has many advantages comparing to the SCM model.

Firstly, the SCM model is based on statistics. Most physical channel parameters are randomly generated statistically following specific distributions. From the statistical point of view, it is acceptable but it does not fit to every scenarios. The real environment has huge impact on the multipath effect especially in indoor scenarios. For indoor-to-outdoor or outdoor-to-indoor scenarios, it does not have support and has not provided any guidance on the statistical distributions of those channel parameters. However in the proposed model, all the physical channel parameters are generated based on the geometrical representation of the scenario and also the real location of the transmitting and receiving antennas. These parameters reflects the impact of real environment.

Secondly, the proposed model has not changed the rasterization mechanism of the IRLA model. The side effect of the rasterization is resolved by a way of rebuilding the multipath components for each pair of antennas although they may in the same rasterization cell. The rasterization mechanism is useful because it has much less computation complexity than vectorised ray launching model. Rays are extremely rich in HetNet environments. The computation complexity between rasterized and vectorised ray launching are significantly different.

Finally, the time-variant character of the new model enables the dynamic system level simulations. The channel behaviour of moving users could be studied with time-variant channel model.

Chapter 4

Performance Evaluations in Indoor Scenario

In this chapter, the proposed model is used to analyse the MIMO system performance in an indoor scenario.

4.1 Introduction

The testing scenario is a building located at Huainan, China. It has 11 stories above ground and one story under ground. Figure 4.1a is a photo of the building. A TD-LTE network has been deployed in the building which is operating at 2300 MHz with 20 MHz bandwidth. It is a distributed MIMO antenna system. The transmitters are deployed on the 1^{st}, 3^{rd}, 7^{th}. The exact locations of the transmitters are illustrated on the screenshots in the following sections. At each transmitting location, there are two antennas. The transmitting power of each antenna is shown as a label next to each antenna which is also visible on those screenshots.

The 3D building model is created in Ranplan iBuildNet as a geometrical representation of the building, see Figure 4.1b. Materials of each building elements, e.g. walls or windows, are picked from the built-in material library from iBuildNet based

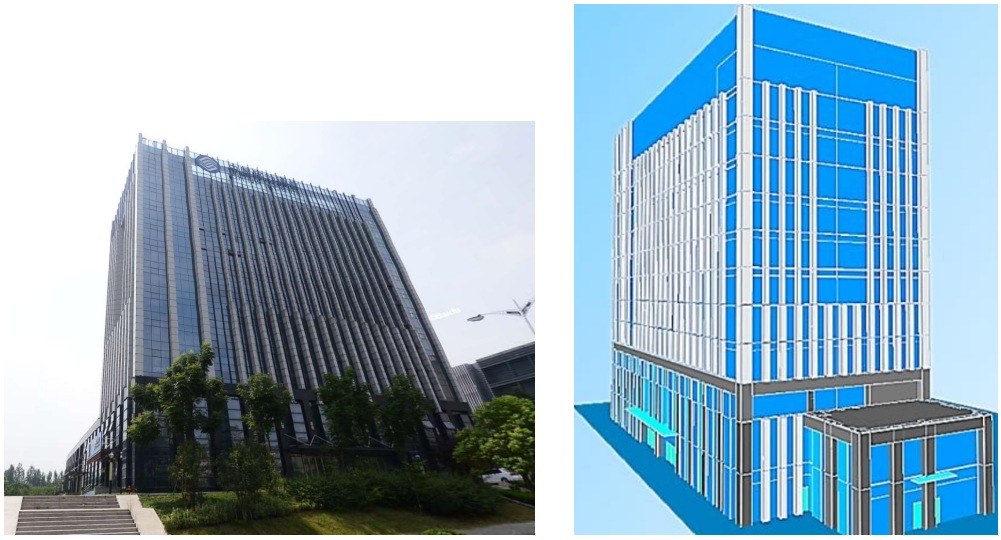

(a) Outside (b) 3D building model

Figure. 4.1 Shannan China Mobile building

Table 4.1 Network and Simulation Parameters

Parameter	Value/Description
Central frequency:	2300 MHz
Total transmitting power:	36 dBm
Transmitter antenna:	pair of omni-directional antennas.
Transmitter antenna separation:	0.5 metre
Transmitter antenna height:	5 metre (1^{st} Floor) 3 metre (other)
MIMO mode:	Space-Frequency Block Coding
Receiver antenna array:	2 linear antennas array
Receiver height:	1 metre
Scheduling algorithm:	ProportionalFair
User profile:	Large file exchange

on the real material used by the building. Based on the current LTE network deployment in the building, the same network is recreated in iBuildNet. The parameters of the deployed network are listed in Table 4.1

There is a built-in simulator in iBuildNet. It is an implementation of the system level simulation algorithm defined by the standard 3GPP 36.814 technical specification [3]. However, the channel model is replaced with the proposed model from Section 3.2.

The simulations are done using a Monte-Carlo method. For each simulation, a thousand of snapshots are generated where each snapshot represents a transmission time interval (TTI) of 100 milliseconds. In each snapshot, 10 users are randomly dropped in the scenario on each floor and each user is assumed to be using heavy data service, which means the full bandwidth is used up.

4.2 MIMO Channel Model Validation

To validate if the proposed MIMO channel model is accurate or not, a set of measurement data is used to compare the simulation results. The measurement campaign was carried out in 2013 by Ranplan using a laptop with a USB dongle that support LTE. The model of the USB dongle is ZTE MF820 and the software used for measurement is ZTE CNT 13.2B2 and ZTE CNA 13.2B2. Three parameters were measured in the campaign including the reference signal received power (RSRP), downlink throughput and SINR. For each measurement location, these parameters are recorded for three minutes and the average is used in the comparison.

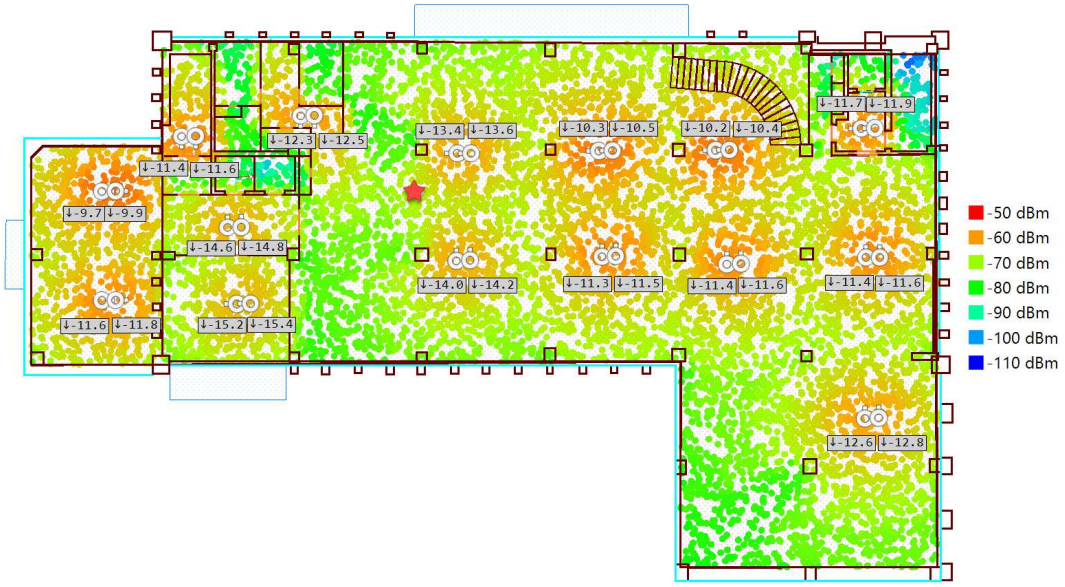

Figure. 4.2 Downlink throughput of each user on the 1st Floor

The first measurement location is on the 1st floor. On this floor, there are 15 transmitting locations. At each transmitting location, there are two antennas. The exact location and transmitting power of these antennas can be seen on Figure 4.2. In the same figure, the RSRP level of each simulated user is also shown as coloured circles. Because there are 1000 snapshots each with 10 user, the Monte-Carlo method has randomly dropped all users over the entire area. The measurement location is indicated by the red star. To compare the simulation results with the measurement data, a simulation user location is picked at the measurement location. The simulated results of those parameters of this user is used to compare with the averaged measurement data. This comparison is shown in Table 4.2. In this table, the measured values of these parameters are averaged over three minutes as described previously. The equipment was put on the measurement location stationary.

Table 4.2 Comparison Result on the 1st Floor

Parameter	Simulation	Measurement
RSRP (dBm):	-67.11	-66.32
Downlink Throughput (Mbps):	74.785	74.056
SINR (dB):	33.17	31.87

From the comparison, it can be see that the simulator with the proposed MIMO channel model shows a good agreement with the measurement data.

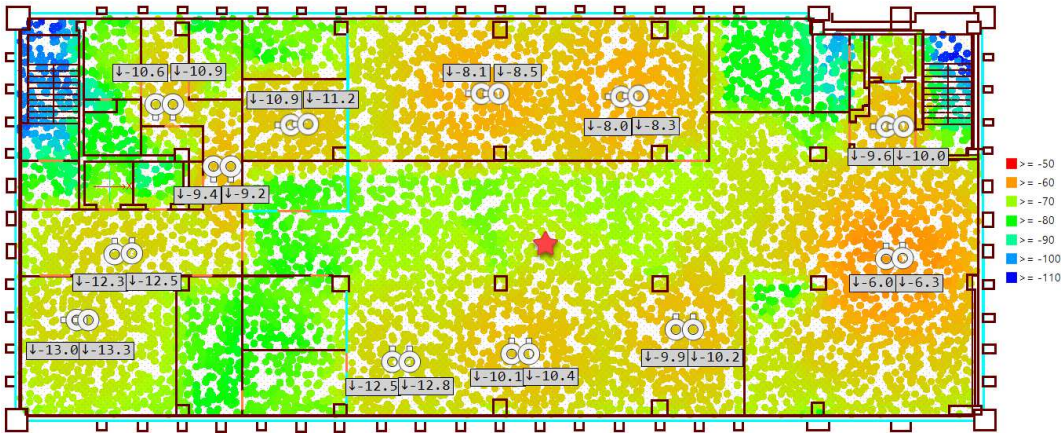

Figure. 4.3 Downlink throughput of each user on the 3rd Floor

The next measurement location is on the 3rd floor and it is indicated by a star on Figure 4.3. There are 12 transmitting locations on this floor. Their locations and output power are also shown on the figure. The RSRP level of each user are illustrated by coloured circles as well. To compare with the measurement data, a simulated user located at the measurement location is also picked. Those three parameters of the selected user are compared with the measurement data in Table 4.3.

Table 4.3 Comparison Result on the 3rd Floor

Parameter	Simulation	Measurement
RSRP (dBm)	-60.30	-60.39
Downlink Throughput (Mbps)	74.51	73.58
SINR (dB)	32.83	29.86

On this floor, the measurement data was taken using the same equipment with the same configurations. All the values are recorded over three minutes and then averaged.

In addition to the above comparison on the average result of those measured parameters, another statistical analyse is performed. The measurement is done at a location on the 7th floor. 560 samples were recorded during the measurement. On this floor, there are 12 transmitting locations. The exact location and the transmitting power of each antenna could be seen on Figure 4.4.

In the simulation tool, a circular region with 0.5 metre radius and the centre of it is set to where the measurement was taken. In the simulation, users are assumed to be within this region and 560 snapshots are generated. The users are randomly dropped in the circular region and they are shown as green dots.

The downlink throughput and the PDSCH SINR are compared between each snapshot and measured sample. The comparisons are illustrated as line graphs in Figure 4.5 and Figure 4.6 respectively. The absolute difference between the simulated value and measured value are also shown on the figures. In Figure 4.5, the absolute

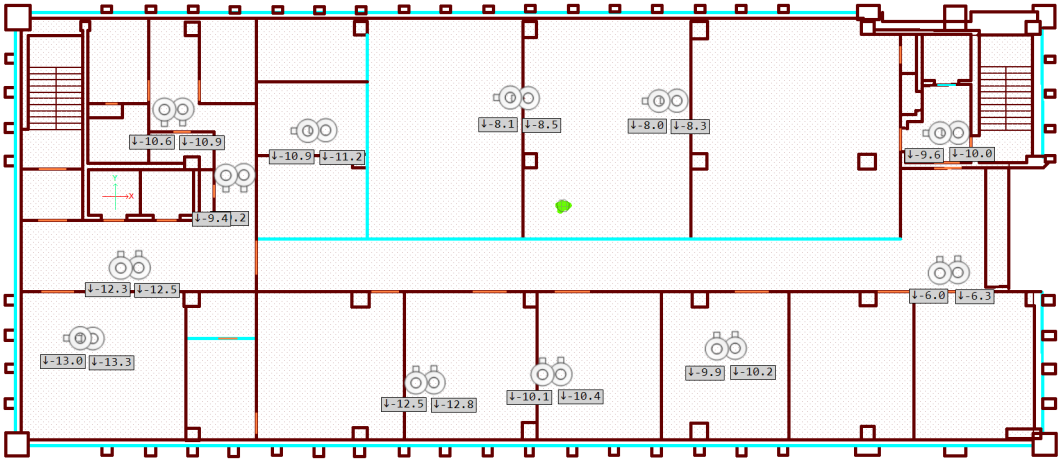

Figure. 4.4 Transmitters and measurement point on the 7th Floor

difference shows that more than 97% samples have less than 3 Mbps error. There are some significant drops on the throughput near sample 230 and 390. These special differences could be caused by moving people during the measurement. In Figure 4.6, The absolute SINR difference is less than 2.5dB at 90% locations and 3dB at 98% locations.

These comparisons shows that the simulator with the proposed MIMO channel model is capable to predict the network performance over time.

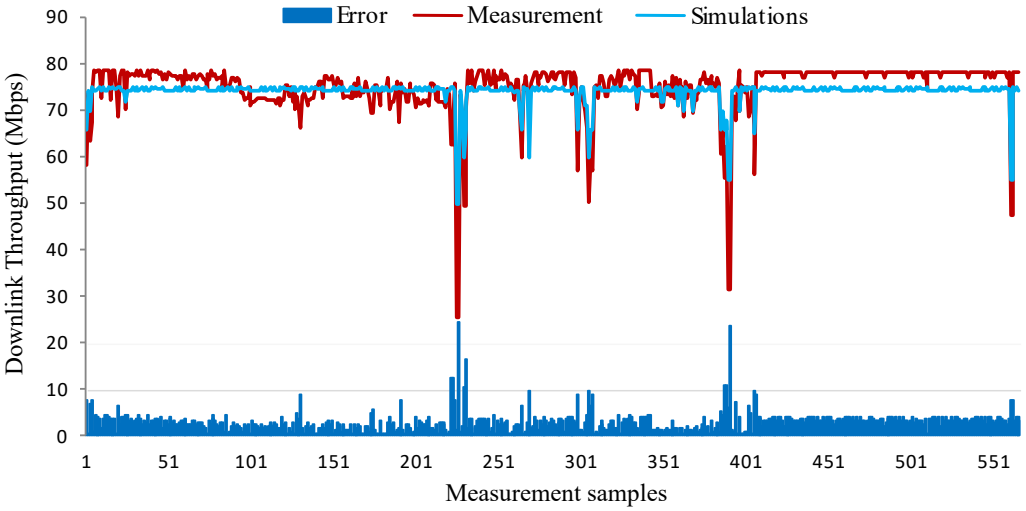

Figure. 4.5 Downlink throughput statistics

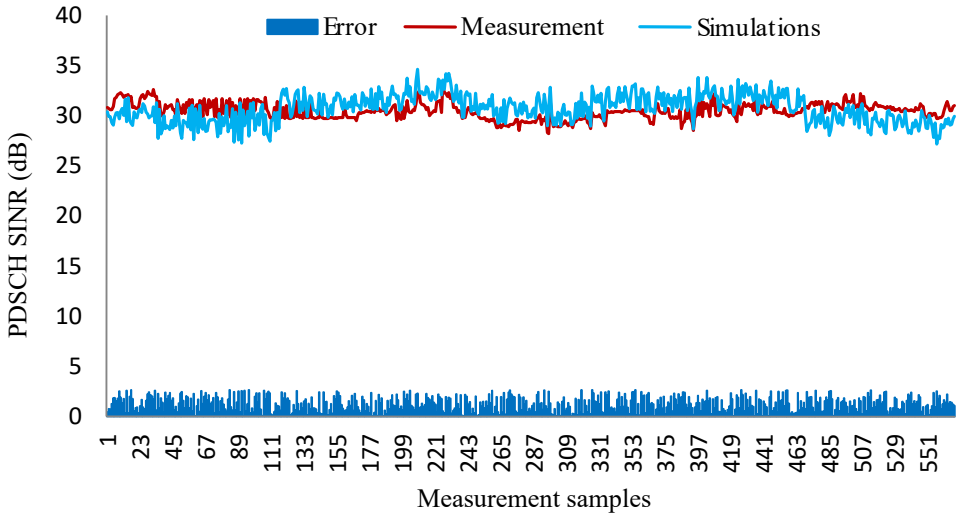

Figure. 4.6 PDSCH SINR statistics

4.3 Summary

In this chapter, the proposed MIMO channel model is used in a LTE network system simulator for generating channel state information. The simulations are run in an indoor building where there is a LTE MIMO system is deployed. For each simulation, the RSRP, downlink throughput and user SINR are generated at randomly placed locations.

The simulation results are compared with measurement data at two locations on the first floor and the third floor. The comparison results show very good agreement between the simulated and measured results. This implies that the proposed model is capable of reflecting the real channel state information so that the simulator could generate such good results.

Additionally, another comparison is carried out by comparing the downlink throughput and PDSCH SINR with hundreds of measurement samples at single location. Both comparisons show that the error is very small over all the samples.

Chapter 5

Conclusions and Future Work

5.1 Conclusions

In this dissertation, the use of a ray optical propagation model, i.e. the IRLA model in MIMO channel modelling is discussed and implemented. A spatial MIMO channel model is then presented and applied in performance evaluations of MIMO systems in real scenario.

The work started with the study of two deterministic propagation models, the IRLA model and the MR-FDPF model. Their performance, in terms of accuracy, computation time and memory consumption are analysed and compared. The comparison results show that both propagation models are capable of predicting signal level coverage accurately, although the MR-FDPF model needs finer resolution to get better predictions. On the contrary, the IRLA model is less sensitive to the resolution but it consumes more computation time than the MR-FDPF model. The memory usage of the MR-FDPF model is roughly twice of the usage by the IRLA model. Taking these factors into account, the IRLA model is ultimately chosen as the propagation model to be used in MIMO channel modelling study.

Next, a spatial MIMO channel model is presented by using the IRLA model. The channel model is similar to the SCM model but the link channel parameters are

deterministically calculated by the propagation model. This gives better prediction of the channel state in specific environments. The channel state between each pair of antennas are rebuilt using a phase shift model which is defined for both linear and circular antenna arrays. This method reduces a great amount of time to calculate multipath between each pair of antennas. In order to extract multipath components from the thousands of rays produced by the IRLA model, a method with a delay threshold is used. The complete MIMO channel model with considerations of polarisation and the Doppler effect is proposed.

Then, the proposed MIMO channel model is used for evaluate the MIMO system performance in an indoor scenario. The result shows that the proposed model is capable for MIMO system analyses. The model is thus validated to be used by network planning tools for modelling MIMO systems.

Although the performance evaluation is done in the specific indoor scenario using a single antenna configuration, the application of the proposed channel model is not just that. For the other antenna configurations, e.g. circular antenna array, the channel model can also be used. Furthermore, the model can also be used in other scenarios after calibrating the material parameters using measurement data. It is not restricted to the specific building as described in the previous chapter.

5.2 Future Work

Although the proposed channel model gives good result in the performance evaluations in the indoor scenario, it is not suitable for millimetre wave (mmWave) band, e.g. 60 GHz. This is because that radio propagation effect at millimetre wave band is much more complicated than lower frequency bands. At mmWave band, the wavelength becomes very short, i.e. 5 millimetre at 60 Ghz. In this case, the diffuse effect on the reflection surface becomes significant. More objects such as ceiling light or furnitures would cause lots of more paths.

When mmWave frequency band is used, it is also possible to use massive MIMO which means using large number of antennas at both ends of the communication link. New methods need to be investigated to rebuild the paths for each pair of antennas.

The proposed model is used in a system level simulator and it is validated at very high level. It is unknown that how it would perform when comparing with other MIMO channel models. This could be another topic to work on in the future.

References

[1] Insoo Hwang, Bongyong Song, and Samir Soliman. A holistic view on hyper-dense heterogeneous and small cell networks. *IEEE Communications Magazine*, 51(6):20–27, jun 2013.

[2] Qualcomm. The 1000x Mobile Data Challenge. *White paper*, (November):1–38, 2013.

[3] 3GPP. Evolved Universal Terrestrial Radio Access (E-UTRA); Further advancements for E-UTRA physical layer aspects. Technical Report 36.814, 2010.

[4] IEEE Std 802.11n-2009; Amendment 5: Enhancements for Higher Throughput. *IEEE-SA Standards Board*, 2009.

[5] P Almers, E Bonek, A Burr, N Czink, M Debbah, V Degli-Esposti, H Hofstetter, P Kyösti, D Laurenson, G Matz, Af Molisch, C Oestges, and H Özcelik. Survey of Channel and Radio Propagation Models for Wireless MIMO Systems. *EURASIP Journal on Wireless Communications and Networking*, 2007(1):019070, 2007.

[6] JP Kermoal and Laurent Schumacher. A stochastic MIMO radio channel model with experimental validation. *Selected Areas in*, 20(6):1211–1226, 2002.

[7] Dimitry Chizhik, Farrokh Rashid-Farrokhi, Jonathan Ling, and Angel Lozano. Effect of antenna separation on the capacity of BLAST in correlated channels. *IEEE Communications Letters*, 4(11):337–339, 2000.

[8] Mérouanne Debbah and Ralf R Müller. MIMO Channel Modeling and the Principle of Maximum Entropy. *IEEE Transactions on Information Theory*, 51(5):1667–1690, 2005.

[9] Akbar M. Sayeed. Deconstructing multiantenna fading channels. *IEEE Transactions on Signal Processing*, 50(10):2563–2579, 2002.

[10] Alvaro Valcarce, Hui Song, and Jie Zhang. Characterization of the Numerical Group Velocity in Yee's FDTD Grid. *IEEE Transactions on Antennas and Propagation*, 58(12):3974–3982, dec 2010.

[11] G De La Roche and Xavier Gallon. On predicting fast fading strength from Indoor 802.11 simulations. *International Conference on Electromagnetics in Advanced Applications (ICEAA)*, pages 407–410, 2007.

[12] GE Athanasiadou and AR Nix. A microcellular ray-tracing propagation model and evaluation of its narrow-band and wide-band predictions. *Selected Areas in Communications, IEEE Journal on*, 18(3):322–335, 2000.

[13] Zhijun Zhang, RK Sorensen, and Zhengqing Yun. A ray-tracing approach for indoor/outdoor propagation through window structures. *Antennas and Propagation, IEEE Transactions on*, 50(5):742–748, 2002.

[14] Lajos Nagy, Róbert Dady, and A. Farkasvolgyi. Algorithmic complexity of FDTD and ray tracing method for indoor propagation modelling. In *Antennas and Propagation, 2009. EuCAP 2009. 3rd European Conference on*, pages 2262–2265. IEEE, 2009.

[15] Mojtaba Dehmollaian and Kamal Sarabandi. Hybrid FDTD and ray optics approximation for simulation of through-wall microwave imaging. In *Antennas and Propagation Society International Symposium 2006, IEEE*, number 1, pages 249–252. IEEE, 2006.

[16] Gunther Auer. 3D MIMO-OFDM channel estimation. *IEEE Transactions on Communications*, 60(4):972–985, apr 2012.

[17] Ramya Bhagavatula, Robert W. Heath Jr, and Kevin Linehan. Performance evaluation of MIMO base station antenna designs. *Antenna Systems and Technology Magazine*, pages 1–15, 2008.

[18] M.a. Jensen and J.W. Wallace. A Review of Antennas and Propagation for MIMO Wireless Communications. *IEEE Transactions on Antennas and Propagation*, 52(11):2810–2824, nov 2004.

[19] Martin Steinbauer, A.F. Molisch, and E. Bonek. The double-directional radio channel. *IEEE Antennas and Propagation Magazine*, 43(4):51–63, 2001.

[20] E. Telatar. Capacity of Multi-antenna Gaussian Channels. *European transactions on telecommunications*, 10(6):585–595, 1999.

[21] G.J. Foschini and M.J. Gans. On limits of wireless communications in a fading environment when using multiple antennas. *Wireless personal communications*, 6(3):311–335, 1998.

[22] Thomas M. Cover and Joy A. Thomas. *Elements of Information Theory*. Wiley & Sons, 1991.

[23] Kai Yu, Student Member, Mats Bengtsson, Björn Ottersten, Darren Mcnamara, Peter Karlsson, and Mark Beach. Modeling of Wide-Band MIMO Radio Channels Based on NLoS Indoor Measurements. *Measurement*, 53(3):655–665, 2004.

[24] J.W. Wallace and M.a. Jensen. Modeling the indoor MIMO wireless channel. *IEEE Transactions on Antennas and Propagation*, 50(5):591–599, may 2002.

[25] A.F. Molisch. A Generic Model for MIMO Wireless Propagation Channels in Macro- and Microcells. *IEEE Transactions on Signal Processing*, 52(1):61–71, jan 2004.

[26] Veli-matti Kolmonen, Katsuyuki Haneda, Tommy Hult, Juho Poutanen, Fredrik Tufvesson, and Pertti Vainikainen. Measurement-Based Evaluation of Interlink Correlation for Indoor Multiuser MIMO Channels. *IEEE Antennas and Wireless Propagation Letters*, 9:311–314, 2010.

[27] Wataru Yamada, Naoki Kita, Motoharu Sasaki, and Takatoshi Sugiyama. Method for Applying Interlink Correlation to Multilink MIMO Propagation Channel Estimation. In *2011 IEEE 73rd Vehicular Technology Conference (VTC Spring)*, pages 1–5. IEEE, may 2011.

[28] Werner Weichselberger and Markus Herdin. A stochastic MIMO channel model with joint correlation of both link ends. *IEEE Transactions on*, 5(1):90–100, 2006.

[29] Nicolai Czink, Bernd Bandemer, G. Vazquez-Vilar, Louay Jalloul, Claude Oestges, and Arogyaswami Paulraj. Spatial separation of multi-user MIMO channels. In *Personal, Indoor and Mobile Radio Communications, 2009 IEEE 20th International Symposium on*, pages 1059–1063. IEEE, 2009.

[30] Sergey L Loyka. Channel capacity of MIMO architecture using the exponential correlation matrix. *IEEE Communications Letters*, 5(9):369–371, 2001.

[31] W. Lee and Y. Yeh. Polarization diversity system for mobile radio. *Communications, IEEE Transactions on*, 20(5):912–923, 1972.

[32] Claude Oestges, Vinko Erceg, and A.J. Paulraj. Propagation modeling of MIMO multipolarized fixed wireless channels. *Vehicular Technology, IEEE Transactions on*, 53(3):644–654, 2004.

[33] J. Hamalainen, Risto Wichman, J.P. Nuutinen, J. Ylitalo, and T. Jamsa. Analysis and Measurements for Indoor Polarization MIMO in 5.25 GHz Band. In *2005 IEEE 61st Vehicular Technology Conference*, volume 1, pages 252–256. IEEE, 2005.

[34] 3GPP. Spatial channel model for Multiple Input Multiple Output (MIMO) simulations. Technical Report 25.996, 2012.

[35] Mansoor Shafi, Min Zhang, Aris L. Moustakas, Peter J. Smith, Andreas F. Molisch, Fredrik Tufvesson, and Steven H. Simon. Polarized MIMO channels in 3-D: Models, measurements and mutual information. *IEEE Journal on Selected Areas in Communications*, 24(3):514–526, 2006.

[36] D S Baum, J Hansen, and J Salo. An interim channel model for beyond-3G systems: extending the 3GPP spatial channel model (SCM). In *2005 IEEE 61st Vehicular Technology Conference*, volume 5, pages 3132–3136 Vol. 5, may 2005.

[37] H. El-Sallabi, D.S. S Baum, Per Zetterberg, Pekka Kyosti, Terhi Rautiainen, and Christian Schneider. Wideband Spatial Channel Model for MIMO Systems at 5 GHz in Indoor and Outdoor Environments. In *2006 IEEE 63rd Vehicular Technology Conference*, volume 6, pages 2916–2921, may 2006.

[38] M Narandzic, Christian Schneider, and R Thoma. Comparison of SCM, SCME, and WINNER channel models. In *Vehicular Technology Conference, 2007. VTC2007-Spring. IEEE 65th*, pages 413–417, 2007.

[39] MF Iskander. Propagation prediction models for wireless communication systems. *Microwave Theory and Techniques, IEEE*, 50(3):662–673, 2002.

[40] M. Hata. Empirical formula for propagation loss in land mobile radio services. *Vehicular Technology, IEEE Transactions on*, 29(3):317–325, aug 1980.

[41] J. Walfisch and H.L. Bertoni. A theoretical model of UHF propagation in urban environments. *Antennas and Propagation, IEEE Transactions on*, 36(12):1788–1796, 1988.

[42] E. Damosso, L.M. Correia, and European Commission. *COST Action 231: Digital Mobile Radio Towards Future Generation Systems : Final Report*. European Commission, 1999.

[43] Zhihua Lai, Guillaume De La Roche, Nik BESSIS, Pierre Kuonen, Gordon Clapworthy, Dibin Zhou, and Jie Zhang. Intelligent ray launching algorithm for indoor scenarios. *Radioengineering*, 20(2):398–408, 2011.

[44] Zhihua Lai, N Bessis, G De laRoche, Hui Song, Jie Zhang, and G Clapworthy. An Intelligent Ray Launching for urban prediction. In *Antennas and Propagation, 2009. EuCAP 2009. 3rd European Conference on*, pages 2867–2871, mar 2009.

[45] S.J. Flores, L.F. Mayorgas, and F.A. Jimenez. Reception algorithms for ray launching modeling of indoor propagation. In *Proceedings RAWCON 98. 1998 IEEE Radio and Wireless Conference (Cat. No.98EX194)*, pages 261–264. IEEE, 1998.

[46] Zhihua Lai and N Bessis. A new approach to solve angular dispersion of discrete ray launching for urban scenarios. *. . . , 2009. LAPC 2009. . . .*, pages 133–136, 2009.

[47] Xiaoming Tu, Hanye Hu, Zhihua Lai, Jean-Marie Gorce, and Jie Zhang. Performance Comparison of MR-FDPF and Ray Launching in an Indoor Office Scenario. In *2013 Loughborough Antennas & Propagation Conference (LAPC 2013)*, Burleigh Court International Conference Centre, Loughborough University, United Kingdom, nov 2013.

[48] Andreas F. Molisch. *Wireless Communications, 2nd Edition*. Wiley-IEEE Press; 2 edition (December 1, 2010), 2002.

[49] Theodore S. Rappaport. *Wireless Communications: Principles and Practice*. Prentice Hall; 2 edition, 2002.

[50] Combined Ray Tracing, Fdtd Method, Modeling Indoor, and Radio Wave. Combined Ray Tracing and FDTD Method for Modeling Indoor Radio Wave Propagation. *Computer*, (x):1668–1671, 1998.

[51] Neil R.S. S Simons, Riaz Siushansian, Joe Lovetri, and Michel Cuhaci. Comparison of the transmission-line matrix and finite-difference time-domain methods for a problem containing a sharp metallic edge. *IEEE Transactions on Microwave Theory and Techniques*, 47(10):2042–2045, 1999.

[52] Jean-Marie Gorce, K. Jaffres-Runser, and G. de la Roche. Deterministic approach for fast simulations of indoor radio wave propagation. *Antennas and Propagation, IEEE Transactions on*, 55(3):938,948, 2007.

[53] G Roche, K Jaffres-Runser, and JM Gorce. On predicting in-building WiFi coverage with a fast discrete approach. *International Journal of Mobile ...*, 2:3–12, 2007.

[54] Zhihua Lai, N Bessis, G de la Roche, P Kuonen, Jie Zhang, and G Clapworthy. On the use of an Intelligent Ray Launching for indoor scenarios. In *Antennas and Propagation (EuCAP), 2010 Proceedings of the Fourth European Conference on*, pages 1–5, apr 2010.

[55] Guillaume De La Roche, Paul Flipo, Guillaume Villemaud, Zhihua Lai, Jie Zhang, and Jean-marie Gorce. Implementation and Validation of a New Combined Model for Outdoor to Indoor Radio Coverage Predictions. *Eurasip Journal on Wireless Communications and Networking*, XXX, 2010.

[56] Rohde-Schwarz. R&S®FSH4 / R&S®FSH8 / R&S®FSH13 / R&S®FSH20 Spectrum Analyzer - Rohde & Schwarz, 2013.

[57] Mitchell Melanie. An introduction to genetic algorithms. *Cambridge, Massachusetts London, England, Fifth printing*, 3, 1999.

[58] D R Jones, C D Perttunen, and B E Stuckman. Lipschitzian optimization without the Lipschitz constant. *Journal of Optimization Theory and Applications*, 79(1):157–181, oct 1993.

[59] Z Lai, N Bessis, and G de LaRoche. An intelligent ray launching for urban prediction. *Antennas and Propagation, 2009. EuCAP 2009. 3rd European Conference on*, pages 2867–2871, 2009.

[60] O. Stabler and Reiner Hoppe. MIMO channel capacity computed with 3D ray tracing model. In *Antennas and Propagation, 2009. EuCAP 2009. 3rd European Conference on*, pages 2271–2275. IEEE, 2009.

Appendix A

Publications

During the course of my MPhil, there are few papers published to conferences and journal. They are listed in this appendix.

1. Tu, X., Hu, H., Lai, Z., Gorce, J.-M., and Zhang, J. (2013). Performance Comparison of MR-FDPF and Ray Launching in an Indoor Office Scenario. In *2013 Loughborough Antennas & Propagation Conference (LAPC 2013)*, Burleigh Court International Conference Centre, Loughborough University, United Kingdom.

2. Tu, X., Weng, J., Salas, S., and Zhang, J. (2014). On the use of an intelligent ray launching in MIMO channel modelling for network planning. In *2014 31th URSI General Assembly and Scientific Symposium, URSI GASS 2014*.

3. Weng, J., Tu, X., Lai, Z., Salous, S., and Zhang, J. (2014). Indoor Massive MIMO Channel Modelling Using Ray-Launching Simulation. *International Journal of Antennas and Propagation*, 2014:1–13.

4. Weng, J., Tu, X., Lai, Z., Salous, S., and Zhang, J. (2015). Modelling the mmWave channel based on intelligent ray launching model. In *2015 9th European Conference on Antennas and Propagation (EuCAP)*, pages 1–4.